A Division of Labor in the Recruitment and Topological Organization of a Bacterial Morphogenic Complex

Paul D. Caccamo[1], Maxime Jacq[1,2], Michael S. VanNieuwenhze[3,4] and Yves V. Brun[1,2] *

[1]Department of Biology, Indiana University, 1001 E. 3rd St, Bloomington, IN 47405, USA

[2]Département de Microbiologie, Infectiologie et Immunologie, Université de Montréal, Pavillon Roger-Gaudry, C.P. 6128, Succursale Centreville, Montréal, Canada

[3]Department of Molecular and Cellular Biochemistry, 212 S. Hawthorne Drive, Indiana University, Bloomington, IN 47405, USA

[4]Department of Chemistry, Indiana University, 800 East Kirkwood Avenue, Bloomington, IN 47405, USA

*** Correspondence: yves.brun@umontreal.ca (Y.V. Brun)**

Abstract

Bacteria come in an array of shapes and sizes, but the mechanisms underlying diverse morphologies are poorly understood. The peptidoglycan (PG) cell wall is the primary determinant of cell shape. At the molecular level, much of the studied morphological variation results from the regulation of PG synthesis enzymes involved in elongation and division. These enzymes are spatially controlled by cytoskeletal scaffolding proteins, such as FtsZ, MreB, and DivIVA, that both recruit and organize the PG synthesis complex. How then do cells define alternative morphogenic processes that are distinct from cell elongation and division? To address this question, we have turned to the specific morphotype of Alphaproteobacterial prosthecae, or "stalks". Stalk synthesis is a specialized form of zonal growth, which requires PG synthesis in a spatially constrained zone to extend a thin cylindrical projection of the cell envelope. The morphogen SpmX defines the site of stalk PG synthesis, but SpmX is a PG

hydrolase. How then does a non-cytoskeletal protein, SpmX, define and constrain PG synthesis to form stalks? Here we report that SpmX and the bactofilin BacA act in concert to regulate stalk synthesis in *Asticcacaulis biprosthecum*. We show that SpmX acts to recruit BacA to the site of stalk synthesis. BacA then serves as a stalk-specific topological organizer that anchors the PG synthesis complex, including its recruiter SpmX, to the base of the stalk, where stalk PG synthesis occurs. In the absence of BacA, cells produce "pseudostalks" that are the result of unconstrained PG synthesis correlated with the mislocalization of SpmX. Finally, we show that BacA is required to inhibit the default function of PG synthesis machinery in cell elongation/division and to prevent DNA entry at the site of stalk synthesis defined by SpmX. Therefore, the protein responsible for recruitment of a morphogenic PG remodeling complex is uncoupled from the protein that topologically organizes the complex.

Introduction

Bacterial cells come in a panoply of shapes and sizes, from the ubiquitous rods and cocci to hyphal, star-shaped, and appendaged bacteria [1]. In addition to shapes that are reproduced faithfully across generations, bacterial cells can dynamically change shape in response to environmental conditions or through a programmed life cycle [1-3]. The shape of most bacteria is determined by the peptidoglycan (PG) cell wall, and the resulting morphology is the product of complex interactions between the proteins and regulatory elements that compose the PG biosynthetic machinery. Much morphological variation results from the differential regulation of divisome or elongasome proteins. For example, the suppression of divisome proteins allows ovococcoid bacteria to form rods under certain biofilm conditions or pathogenic rod-shaped bacteria to filament during infection [3-6]. Filamentous Streptomycetes form branching hyphae by localizing the same elongation machinery in different places [3, 7]. How then do cells define a new morphological process that is distinct from the elongasome or divisome, but still operates in the context of those critical PG synthesis modes? To address this question, we have turned to the specific morphotype of Alphaproteobacterial prosthecae.

Prosthecae, or “stalks,” are non-essential extensions of the bacterial cell body thought to play a role in nutrient uptake [8, 9]. Stalk synthesis requires PG synthesis in a spatially constrained zone in order to extend a thin cylindrical projection of the cell envelope. The stalk is compartmentalized from the cytoplasm, as it is devoid of DNA and ribosomes and excludes even small cytoplasmic proteins such as GFP [9]. *Asticcacaulis biprosthecum*, a gram negative Alphaproteobacterium from the Caulobacteraceae family [10], produces two bilateral stalks whose synthesis depends on PG synthesis at the base of the incipient stalk structures (red arrows in Figure 1A)

[11]. How do cells harness PG synthesis machinery to produce stalks while preventing its typical function of cell elongation or division?

Here we report how a recently identified class of bacterial cytoskeletal protein, known as "bactofilin", plays a dual role by defining the topography of PG synthesis for the synthesis of stalks and by inhibiting a default cell elongation mode at that same site in *A. biprosthecum*. Bactofilins are conserved throughout the bacterial kingdom and are characterized by the presence of a central conserved DUF583 (or "bactofilin") domain flanked by N- and C-terminal regions of variable length and sequence (Figure 1B) [12]. Bactofilins are involved in cell shape determination in a number of species. For example, in the helical *Helicobacter pylori* and *Leptospira biflexa*, bactofilins are required for proper helical shape generation [13, 14]. In *Caulobacter crescentus*, bactofilins optimize the rate of stalk synthesis at the cell pole by a yet unknown mechanism [12]. It is not well understood how bactofilins exert an effect on morphology, but a common theme appears to be association or direct interaction with PG modifying enzymes.

The best studied bacterial cytoskeletal proteins (MreB, FtsZ, and DivIVA) serve dual roles as both recruiters and organizers of the proteins for their respective PG synthesis complexes. In contrast, we show that the roles of recruiter and organizer of PG synthesis have undergone a division of labor in *A. biprosthecum* stalk synthesis, where a morphogen recruits its own organizing cytoskeletal protein. Our prior work established that the recruitment of the stalk PG synthesis machinery is performed by the modular morphogen SpmX: changing SpmX location is sufficient to drive stalk synthesis at a new site [11], much like changing the position of FtsZ changes the location of the site of

cell division. However, SpmX is a PG hydrolase, not a cytoskeletal protein [11, 15]. How then does a non-cytoskeletal protein, SpmX, define and constrain PG synthesis to form stalks? In this work, we identify the cytoskeletal scaffolding protein that provides topological specificity to the stalk synthesis machinery, including to the recruiter SpmX itself. We apply genetics, cell biology, microscopy, chemical labeling, and quantitative analysis to examine the interconnected roles of the morphogen SpmX and the bactofilin BacA in *Asticcacaulis biprosthecum* stalk synthesis. We present evidence that SpmX and BacA act in a coordinated fashion to initiate and regulate stalk synthesis. SpmX acts as the recruiter of the stalk synthesis complex, including BacA. BacA then serves as a stalk-specific cytoskeletal scaffolding protein that anchors the putative synthesis complex, including SpmX, to the base of the stalk, and defines the width of the complex. In the absence of BacA, cells produce abnormal "pseudostalks" that are the result of unconstrained PG synthesis correlated with the mislocalization of SpmX. Finally, we show that BacA is required to block entry of the PG synthesis machinery involved in cell elongation and division, as well as DNA, from the site of stalk synthesis defined by SpmX. Therefore, the protein responsible for recruitment of a morphogenic PG remodeling complex is uncoupled from the protein that topologically organizes the complex. Such decoupled recruitment and scaffolding processes may prove more versatile for morphogenetic events that do not simply involve modulation of cell elongation or division.

Results

A. biprosthecum encodes a single bactofilin gene whose product self-polymerizes *in vitro*

A. biprosthecum has proven to be a better system than *C. crescentus* to identify genes required for stalk synthesis because: 1) The *A. biprosthecum spmX* mutant is the only known stalkless mutant in any Caulobacterales species whose phenotype is not bypassed by phosphate starvation [11, 16, 17], which stimulates stalk synthesis [11, 18-20]; 2) *A. biprosthecum* stalks are located at midcell, away from the myriad of polarly localized proteins involved in *C. crescentus* development and cell cycle progression [21-24], eliminating any potentially confounding co-localization or interaction data; and 3) many of the genetic tools developed for *C. crescentus* work in *A. biprosthecum*. In *C. crescentus*, deletion of the bactofilin genes *bacA* and *bacB* (for clarity, these will be referred to as "$bacA_{Cc}$" and "$bacB_{Cc}$") leads to a slight reduction in length of otherwise normal stalks [12, 25, 26]. Only $bacA_{Cc}$ has a homolog in the *A. biprosthecum* genome, which we have named "*bacA*" (Figure 1C). The genomic arrangement of the *A. biprosthecum bacA* locus is similar to that of *C. crescentus* $bacA_{Cc}$, with a putative M23 family metallopeptidase gene (CC1872/ABI_34190) directly upstream and overlapping the $bacA_{Cc}$/*bacA* coding regions, and a putative peroxiredoxin gene (CC1871/ABI_34200) further upstream (Figure 1C). BacA exhibits high sequence and predicted structural similarity to the *C. crescentus* bactofilins, with a central DUF583 domain composed of repeating β strands flanked by proline-rich N- and C-termini, suggesting similar biochemical properties (Figure 1D). Indeed, $BacA_{Cc}$ can self-assemble *in vitro* into filaments, filament bundles, and sheets [12, 27]. To test if *A. biprosthecum* BacA is an auto-polymerizing protein, we overexpressed and purified both $BacA_{Cc}$ and BacA in *Escherichia coli* and visualized the purified proteins via

transmission electron microscopy (TEM) (Figure 1E). While $BacA_{Cc}$ readily polymerized in various environments (salt, pH, chaotropic agent), under similar conditions BacA formed proteins aggregates instead of filaments. While most conditions tested did not improve BacA solubility, addition of high detergent concentration (10% Triton X-100) allowed filament formation. The TEM micrographs show that both bactofilin proteins, $BacA_{Cc}$ and BacA, self-polymerize *in vitro* to form protofilament bundles, with BacA forming 90 nm wide filaments made of single filaments stacked together through lateral-lateral interactions, similar to $BacA_{Cc}$ (Figure 1E).

BacA is required for stalk synthesis

In *C. crescentus*, deletion of the bactofilin homologs $bacA_{Cc}$ and/or $bacB_{Cc}$ does not abrogate stalk synthesis or impact stalk ultrastructure, but results in a slight reduction in stalk length under stalk synthesis-stimulating phosphate-limited conditions [12]. This suggests that, in *C. crescentus*, deletion of $bacAB_{Cc}$ affects only stalk longitudinal extension and to a limited extent [12]. Strikingly, ~95% of *A. biprosthecum* Δ*bacA* mutant cells were completely stalkless when grown in the complex medium PYE, with a small proportion of cells exhibiting bump-like protrusions at the midcell where stalks would normally be found (Supplemental Figure 1). Since growth in rich medium may mask latent stalk phenotypes [11, 20], the Δ*bacA* mutant was studied under phosphate starvation, which stimulates stalk synthesis [11, 18-20], to study the Δ*bacA* mutant. In low phosphate medium, more than half (58% ± 12%) of WT cells possessed a visible cell body extension, all of which were stalks (Figure 2). In the Δ*bacA* mutant, only 3% ± 2% of total cells produced a stalk (Figure 2). Instead of synthesizing stalks, the Δ*bacA* mutant produced short, wide protrusions at the bilateral positions where stalks are normally synthesized, which we termed “pseudostalks” (Figure 2A and red arrows in

Figure 2B). Under phosphate starvation, the stalks produced by WT cells were 7.3 ± 3.7 µm long and 171 ± 13 nm in diameter at the base (Figure 2). Pseudostalks were significantly shorter than stalks at 0.9 ± 0.5 µm long (~88% decrease in length compared to WT), were more variable in diameter, and were often branched or "frazzled" at the ends (Figure 2). Pseudostalks were significantly wider in diameter at the base, 392 ± 73 nm or an ~129% increase in width compared to WT (Figure 2).

The presence of a low-copy plasmid encoding *bacA* expressed from the native promoter restored stalk synthesis, albeit partially, in the Δ*bacA* mutant. Complemented Δ*bacA* cells produced stalks 2.4 ± 2.0 µm long that, while shorter than WT stalks, were significantly longer than Δ*bacA* pseudostalks (Figure 2). In addition, 28% ± 6% of complemented Δ*bacA* cells produced WT-like stalks, a significant increase over the mutant (Figures 2). Both stalk diameter and variability in stalk diameter (178 ± 20 nm) were restored to WT levels in the complemented Δ*bacA* cells (Figure 2). Taken together, these data show that BacA is required for stalk synthesis in *A. biprosthecum*.

BacA localizes to the site of stalk synthesis after SpmX localization

While the localization of SpmX is known, the pattern of BacA localization is not. The stalk morphogen SpmX localizes to the future site of stalk synthesis in predivisional cells of *Asticcacaulis*, where it marks the site of stalk synthesis, which occurs after cell division and swarmer cell differentiation in the next cell cycle [11] (Figure 3A). To investigate the subcellular localization of BacA in WT cells, we fused BacA to mVenus at the native locus and performed fluorescence microscopy.

We first performed time-lapse fluorescence microscopy of BacA-mVenus to determine the timing of BacA localization relative to that of SpmX (Figure 3B and Supplemental

Movie 1). The first four panels of Figure 3B (0-84 min) show the elongation of a predivisional mother cell as it produces an incipient swarmer daughter cell, where BacA is already localized at bilateral positions in the stalked half of the cell. After cell division (the transition from 84-112 min), a BacA-mVenus focus appeared at a lateral position in the incipient swarmer cell. While only one BacA-mVenus focus is visible in the overlay from 112 to 140 min, a second focus is clearly visible in the overlay at 168 and 196 min. This process of BacA localization after cell division is repeated in later panels with a second daughter cell (140-252 min). Therefore, SpmX localizes first in predivisional cells where it marks the sites of stalk synthesis, followed by BacA localization after cell division. We then sought to quantify BacA-mVenus localization at the population level, rather than single cells. Overall, BacA-mVenus localized to bilateral positions at the base of the stalks (Figure 3C). A population-level heatmap of the subcellular localization of BacA-mVenus foci exhibited a localization pattern similar to that of SpmX [11], with foci clustering in a bilateral manner at the midcell (Figure 3D).

SpmX is required for BacA localization

Considering that 1) both SpmX and BacA are required for WT stalk synthesis; 2) that both proteins localize to the site of stalk synthesis; and 3) that SpmX localizes to the site of stalk synthesis prior to BacA, we hypothesized that SpmX is required for BacA localization. In order to test the role of SpmX in BacA localization, we constructed a strain with *bacA-mVenus* fusion at the native locus in the Δ*spmX* background (Figure 3C-3F).

As reported above in the WT background, BacA-mVenus localized to the base of the stalk (Figure 3C) with foci clustering in a bilateral manner at the midcell (Figure 3D). In

the Δ*spmX* mutant, BacA-mVenus was often mislocalized toward the poles (Figure 3C), and the population-level heatmap of the subcellular localization of BacA-mVenus foci in the Δ*spmX* mutant showed that BacA-mVenus was randomly distributed throughout the cell body (Figure 3D). To further investigate BacA-mVenus dynamics in WT and Δ*spmX* strains, we performed time-lapse fluorescence microscopy (Supplemental Movies 1 & 2) and used particle tracking to track movement and velocity changes for individual foci (Figure 3E & 3F). In WT cells, BacA-mVenus foci were constrained bilaterally at sites of stalk synthesis and remained relatively static once they appeared (Figure 3B, 3E, & 3F and Supplemental Movie 1). Conversely, in the Δ*spmX* mutant, BacA-mVenus foci moved randomly throughout the cell body and exhibited start-stop patterns of spikes and drops in velocity (Figure 3E & 3F and Supplemental Movie 2). Taken together, these data show that SpmX is required for BacA localization.

BacA and SpmX interact in a bacterial two-hybrid system

Since SpmX is required for BacA localization, we tested whether SpmX and BacA interact *in vivo* using bacterial adenylate cyclase two-hybrid (BACTH) assays [28] (Figure 4). We tested all combinations of T18 and T25 fusions for SpmX and BacA. Both SpmX and BacA showed self-interactions (Figure 4), consistent with previous results showing that *C. crescentus* SpmX forms oligomers [29] and confirming our results showing BacA is a self-polymerizing protein (Figure 1E). Notably, we also observed SpmX-BacA interactions (Figure 4C & 4D), although the only interactions we observed were when BacA was fused with the T25 fragment on the N-terminus (T25-BacA). These results make sense in the context of recent work showing that the N-terminal tail of *Thermus thermophilus* bactofilin is required for membrane binding [30]. If the BacA N-terminal tail is also involved in membrane binding, the fact that we only

detect SpmX-BacA interactions when the C-terminal tail is unencumbered by a fusion suggests that the C-terminal region of BacA is involved in protein-protein interactions with SpmX.

BacA is required to stabilize SpmX to the stalk base

Cytoskeletal scaffolding proteins can be loosely defined as proteins that physically organize the molecular components of a biological process or pathway [3]. Because 1) SpmX acts in a modular fashion to define the site of stalk synthesis [11]; 2) is required for BacA localization; and 3) BacA is required to constrain stalk diameter, we hypothesized that BacA organizes PG synthesis enzymes, and perhaps SpmX, at the site of stalk synthesis. To test SpmX localization in the absence of BacA, we constructed strains with *spmX-eGFP* fusions at the native locus in both WT and Δ*bacA* backgrounds. Consistent with previously published results [11], fluorescence microscopy showed that SpmX-eGFP localizes bilaterally to the site of stalk synthesis in WT cells (Figures 5A & 5B). Interestingly, SpmX localized to the nominal site of stalk synthesis even in the absence of BacA (Figures 5A & 5B). However, SpmX-eGFP often localized to the tips of the pseudostalks of the Δ*bacA* mutant, rather than the base as it does in WT cells (Figure 5A & 5B). This defect of SpmX localization is further revealed by the localization heatmaps, where, rather than a tight localization close to the cell envelope in WT, there is a diffuse localization at the midcell that radiates away from the cell body in the *bacA* mutant (Figure 5B). Indeed, quantification of the orthogonal distance of SpmX-eGFP maxima from the medial axis of the associated cell, showed a significant increase in Δ*bacA* cells compared to WT (Figure 5C). In addition, both the area of the SpmX-eGFP maxima (Figure 5D) and the relative fluorescence intensity (Figure 5E) significantly increased in the Δ*bacA* mutant compared to WT, suggesting

that regulation of SpmX organization and protein levels are disrupted. Taken together with the BACTH results, these results indicate a scaffolding role for BacA during stalk synthesis whereby BacA is required to stabilize and constrain SpmX in a tight area at the base of the stalk.

Pseudostalks are composed of PG and formed through delocalized PG synthesis

A. biprosthecum stalks extend through the addition of newly synthesized PG at the base of the stalk and are composed of PG throughout [11]. We wanted to test if the short, wide pseudostalks of the Δ*bacA* mutants were the result of unconstrained PG synthesis, albeit at the proper bilateral positions. It has been shown that isolated PG sacculi maintain the shape of the bacterial cell, including PG-containing stalks [31]. To test if pseudostalks are composed of PG, we first isolated sacculi from *A. biprosthecum* WT and Δ*bacA* cells. As expected, *A. biprosthecum* WT sacculi exhibited long and thin bilateral extensions of stalk PG (Figure 6A). Sacculi purified from Δ*bacA* cells showed sac-like bilateral extensions of PG that mimicked the morphology of pseudostalks (Figure 6A), confirming that pseudostalks are composed of PG.

There are several modes of PG synthesis that could result in pseudostalks. For example, they could be synthesized 1) from the base like WT stalks, albeit with a wider and variable area of extension; 2) via polar growth similar to vegetative growth of the filamentous Streptomycetes [3], with PG remodeling occurring through polar tip extension; or 3) be the result of dispersed PG synthesis throughout the pseudostalk, similar to lateral elongation of some rod-shaped cells [3].

To test these possibilities, we employed various methods of Fluorescent D-Amino Acid (FDAA) [32] labeling to visualize active PG synthesis during growth in low-phosphate

medium. Cells were first subjected to pulses (45 min or ~20% of doubling time) of a red FDAA (TADA) (Figure 6B). If pseudostalks are synthesized from the base, the FDAA should label the cell, but not the pseudostalk itself. In WT cells, labeling was diffuse throughout the cell, but absent from the stalks (Figure 6B), consistent with previous results [11]. In contrast, Δ*bacA* cells showed strong labeling throughout the pseudostalks, indicating that these structures are not synthesized from the base as in WT stalks (Figure 6B). To obtain better spatiotemporal resolution of PG remodeling and to correlate SpmX localization with PG remodeling, we performed virtual time-lapse FDAA labeling [32], where short successive pulses of different colored FDAA probes are used for spatiotemporal labeling of areas of PG synthesis. *A. biprosthecum* WT SpmX-eGFP and Δ*bacA* SpmX-eGFP cells were first labeled with a blue FDAA (HADA) for 6 min followed by a red FDAA (TADA) for 3 min, with the dye being washed away after each respective incubation (Figure 6C). Cells were then imaged via 3D-SIM (Structured Illumination Microscopy). For WT cells, the HADA and TADA signals overlapped both in the cell body and at the base of the stalk, colocalized with the SpmX-eGFP focus and consistent with stalk PG synthesis at the base and no PG synthesis along the stalk length (Figure 6C). In contrast, the HADA and TADA signals overlapped in both the cell body and the pseudostalks of Δ*bacA* cells and SpmX-eGFP localizing to the tips of the pseudostalks (Figure 6C), indicating that pseudostalks are formed via dispersed PG synthesis throughout the structure.

BacA inhibits the default elongation and division modes of PG synthesis as well as DNA entry at sites of stalk synthesis

While the FDAA labeling techniques used above (Figure 6B & 6C) show that new PG is incorporated into the pseudostalk, it does not distinguish *per se* if PG is being incorporated from the base, as in WT stalks, or if PG incorporation is distributed throughout the pseudostalk. To determine the PG incorporation pattern for Δ*bacA* pseudostalks, we performed pulse-chase FDAA labeling (Figure 6D). *A. biprosthecum* WT and Δ*bacA* cells were first labeled with a red FDAA (TADA) to ensure whole-cell labeling, including stalks and pseudostalks. Cells were then washed twice to remove the FDAA and time-lapse fluorescent microscopy was performed. As the *A. biprosthecum* WT cells grew, FDAA signal disappeared from the cell body, but was retained in the stalk (Figure 6D), with a slight clearing near the base as stalk PG was synthesized from its base (Figure 6D, yellow triangles). In contrast, Δ*bacA* cells lost FDAA signal throughout both the cell body and the pseudostalks at a similar rate (Figure 6D), consistent with PG synthesis throughout the pseudostalk. Strikingly, 49% (42/85) of Δ*bacA* cells observed were able to extend and divide from the pseudostalks and produced cell-like extensions that continued to elongate after cytokinesis (yellow triangles in Figure 6E), suggesting that cell growth was occurring at sites usually reserved for stalk synthesis. These results suggested that BacA might be required to prevent entry of chromosomal DNA that would be required for continued growth of these lateral cell extensions. To determine if Δ*bacA* pseudostalks contained DNA, we stained live cells with DAPI. In WT cells, DAPI staining was constrained to the cell body, but in Δ*bacA* cells, pseudostalks stained strongly for DNA (Figure 6F). It should be noted that

we were unable to determine the viability of the cell-like structures produced from the pseudostalks, but, qualitatively, there is no discernable difference between the growth of WT and Δ*bacA* strains in liquid culture or on plates. Taken together, these data indicate that, in addition to providing a scaffold for proper stalk PG synthesis at its base, BacA inhibits not only unwanted PG synthesis involved in cell elongation and division, but also the entry of DNA at sites of stalk synthesis.

Discussion

Intricate biological processes underlie even the simplest of shapes. The ubiquitous rod- and sphere-shaped bacteria can be generated through multiple strategies [33, 34], but the final observed form is the result of finely tuned gene expression, metabolic processes that regulate PG precursor and subunit levels, and the spatiotemporal localization of PG-modifying enzymes. The study of shape generation and maintenance has uncovered a common theme of scaffolding proteins such as MreB, FtsZ, and DivIVA that recruit and organize PG synthesis to specific subcellular locations at specific times. Here we present evidence that the paradigm of a cytoskeletal scaffolding protein serving the dual roles of recruitment and organization in PG synthesis is not always true. In *A. biprosthecum*, the roles of recruitment and organization for the stalk synthesis PG remodeling complex are performed by two distinct proteins, SpmX and BacA, respectively. Furthermore, BacA prevents the cell elongation and division PG synthesis machinery from being activated at the site of stalk PG synthesis. Finally, BacA also prevents the entry of DNA into stalks.

Previous work has shown that SpmX appears early in *Asticcacaulis* spp. cell cycle, where it localizes in pre-divisional daughter cells to mark the future site of stalk synthesis [11]. Here we show that BacA operates downstream of SpmX for subcellular localization in the *A. biprosthecum* stalk synthesis pathway but acts upstream of SpmX for the topological organization of SpmX and the PG synthesis machinery. In the absence of SpmX, cells are stalkless and BacA-mVenus forms foci that move randomly throughout the cell body, indicating that SpmX recruits BacA, and presumably other PG remodeling enzymes that remain to be discovered, to the site of stalk synthesis (Figure 7A). Once stalk synthesis is initiated, BacA serves as a scaffolding protein that

constrains PG synthesis at the base of the stalk, allowing for WT stalk elongation and maturation (Figure 7A). Based on current knowledge, this is the first reported morphogenic PG remodeling process in which the proteins responsible for recruitment of the complex are decoupled from the scaffolding proteins that organize the complex. Such decoupled recruitment and scaffolding processes may prove more versatile for morphogenetic events that do not simply involve modulation of cell elongation or division.

Many questions remain regarding prosthecae synthesis in both *A. biprosthecum* specifically and the stalked Alphaproteobacteria in general. Even among closely related species there are phenotypic differences, such as the number and placement of stalks, as well as differences in the genes involved in stalk synthesis. Furthermore, in many stalked marine species, the stalk serves a reproductive function, with a budding daughter cell produced from the tip of the stalk [35-38]. How have these stalk synthesis pathways evolved? Are there core genes that are shared amongst bacteria that produce stalks? There are certainly differences, specifically between *C. crescentus* and *A. biprosthecum* (Supplemental Table 1) [11], but what other genes are involved in *A. biprosthecum* stalk synthesis? ABI_34190, the gene that lies upstream and overlaps *bacA* (Figure 1C), is a putative M23 family metallopeptidase (Pfam 01551) whose predicted endopeptidase activity would cleave PG crosslinks. Thus, ABI_34190 provides an intriguing candidate for both its predicted function in PG remodeling and its genomic association with *bacA*. How do bactofilins function in stalk synthesis? Presumably, the ability to self-polymerize is important to bactofilin function in general but, to date, there have been no studies showing that non-polymerizing mutants lead to

a phenotypic change. The terminal regions flanking the conserved bactofilin domain often vary between species. Do the N- and C-terminal domains serve any specific purposes? Work on *T. thermophilus* bactofilin showed that the N-terminal region is involved in membrane binding [30]. We used high detergent levels, a high micellization condition, to get purified BacA to form filaments *in vitro*. Our BACTH results suggest that the C-terminus is important for BacA-SpmX interaction. It seems likely that these N- and C- terminal regions play important roles in membrane and protein interactions.

This study has also revealed an unexpected role for a scaffold protein in inhibiting default modes of PG synthesis. In the absence of BacA, cells produce what we have termed "pseudostalks", which are significantly shorter and wider than stalks. In addition, BacA is required to stabilize SpmX at the base of the stalk (Figure 7A), as observed by the mislocalization of SpmX-eGFP in the absence of BacA (Figure 7B). Pseudostalks, like WT stalks, are composed of PG. However, unlike WT stalks, which are synthesized from the base of the stalk (Figure 7A), pseudostalks are the result of dispersed PG remodeling throughout the structure (Figure 7B). We find a parallel for this phenomenon with the cytoskeletal scaffolding protein DivIVA in the Actinobacterium *Mycobacterium smegmatis*. Normal, rod-shaped *M. smegmatis* undergo asymmetric bipolar growth, and DivIVA focuses this cell envelope assembly at the poles [39]. When DivIVA is depleted, PG synthesis persists, but in a disorganized manner throughout the cell, leading to spherical cells [40]. Similarly, in the absence of BacA, PG synthesis persists, but in a disorganized manner leading to pseudostalks.

Strikingly, we show that the pseudostalks that form in the absence of BacA can incorporate the default cell elongation and cell division modes, forming cell body

extensions that contain DNA and can divide. These results suggest that the cytoskeletal bactofilin BacA not only organizes and constrains PG synthesis to specific subcellular locations (Figure 7A) but, also inhibits the default function of PG synthesis machinery in cell elongation and division and DNA entry at the site of stalk synthesis defined by SpmX. The decoupling of the recruitment and scaffolding roles for proteins that localize the PG synthesis complex may facilitate safeguarding against establishment of cell elongation and division at those morphogenetic sites. However, removal of a single layer of regulation (in this case, *A. biprosthecum* BacA) can lead to unregulated growth, with *A. biprosthecum* becoming a branching organism via pseudostalks. This follows an emerging theme of bacterial morphogenesis in which morphological variation results from the differential regulation of PG remodeling [3, 41, 42]. In other words, much like the Actinobacteria *Streptomyces* spp., *A. biprosthecum* localizes PG synthesis at specific places with different morphological results: branching hyphae and stalks, respectively. Furthermore, this result suggests that at least some of the PG synthesis enzymes used for stalk synthesis are the same as those used for cell elongation and division, which may explain why we have yet to identify a PG synthesis enzyme used specifically for stalk synthesis.

Methods

Bacterial strains and growth conditions

All freezer stocks were maintained in 10% DMSO at -80°C.

A. biprosthecum strains used in this study were grown in liquid PYE medium at 26°C supplemented with antibiotics or supplements as necessary (kanamycin 5 µg ml^{-1}, gentamycin 0.5 µg ml^{-1}, spectinomycin 25 µg ml^{-1}, streptomycin 5 µg ml^{-1}, and 0.3 mM diaminopimelic acid). Strains were maintained on PYE plates at 26°C supplemented with antibiotics or supplements as necessary (kanamycin 5 or 20 µg ml^{-1}, gentamycin 2.5 µg ml^{-1}, spectinomycin 50 µg ml^{-1}, streptomycin 20 µg ml^{-1}, 3% sucrose, and 0.3 mM diaminopimelic acid). For phosphate starvation, cells were grown in Hutner base-imidazole-buffered-glucose-glutamate (HIGG) medium [43] containing 30 µM phosphate (phosphate-limited), supplemented with biotin at 40 ng ml^{-1} and antibiotics where appropriate. For microscopy of PYE grown samples, strains were inoculated in PYE from colonies and grown at 26°C with shaking until mid- to late-exponential phase ($OD_{600} \geq 1.0$) before imaging. For microscopy of HIGG grown, phosphate-limited samples, strains were inoculated in PYE from colonies and grown at 26°C with shaking until late-exponential phase. Cultures were then washed 2X with deionized distilled H_2O (ddH_2O), diluted 1:20 in HIGG, and grown at 26°C with shaking for 72h before imaging.

E. coli strains used in this study grown in liquid lysogeny broth (LB) medium at 37°C (or 30°C for BACTH assays) supplemented with antibiotics or supplements as necessary (ampicillin 100 µg ml^{-1}, kanamycin 30 µg ml^{-1}, gentamycin 15 µg ml^{-1}, spectinomycin 100 µg ml^{-1}, streptomycin 30 µg ml^{-1}, 0.3 mM diaminopimelic acid, and X-gal 40 µg ml^{-1}). Strains were maintained on LB plates at 37°C (or 30°C for BACTH assays) supplemented with antibiotics or supplements as necessary (ampicillin 100 µg ml^{-1},

kanamycin 25 or 50 µg ml^{-1}, gentamycin 20 µg ml^{-1}, streptomycin 30 or 100 µg ml^{-1}, 0.3 mM diaminopimelic acid (DAP), X-gal 40 µg ml^{-1}, and 0.5 mM IPTG).

Electroporation of *A. biprosthecum* was performed as previously described [44]. Outgrowth was performed for 8-24h at 26°C. For electroporation with replicating plasmids, 100 µl of outgrowth culture was plated on PYE plates with appropriate selection at dilutions of 10^1, 10^0, and 10^{-1}. For electroporation with integrating plasmids, outgrowth was divided into volumes of 100, 300, and 600 µl and plated on PYE plates with appropriate selection.

In-house stocks of chemically competent BL21lDE3 (YB1000), DAP auxotroph WM3064 (YB7351), XL-1 Blue (YB0041), and BTH101 (YB9171) *E. coli* cells were prepared as previously described [45, 46].

Recombinant DNA Methods

DNA amplification, Gibson cloning, and restriction digests were performed according to the manufacturer. Restriction enzymes and Gibson cloning mix were from New England Biolabs. Cloning steps were carried out in *E. coli* (alpha-select competent cells, Bioline or XL1-Blue, Stratagene) and plasmids were purified using Zyppy Plasmid Kits (Zymo Research Corporation). Sequencing was performed by the Indiana Molecular Biology Institute and Eurofins MWG Operon Technologies with double stranded plasmid or PCR templates, which were purified with a DNA Clean & Concentrator kits (Zymo Research Corporation). Chromosomal DNA was purified using the Bactozol Bacterial DNA Isolation Kit (Molecular Research Center).

Plasmids were introduced into all *E. coli* strains using chemical transformation according to the manufacturer's protocols. Electroporation of *A. biprosthecum* was

performed as previously described [44]. Outgrowth was performed for 8-24h at 26°C. For electroporation with replicating plasmids, 100 µl of outgrowth culture was plated on PYE plates with appropriate selection at dilutions of 10^1, 10^0, and 10^{-1}. For electroporation with integrating plasmids, outgrowth was divided into volumes of 100, 300, and 600 µl and plated on PYE plates with appropriate selection. Mating of plasmids into *A. biprosthecum* was performed using the *dap*$^-$ *E. coli* strain WM3064 (YB7351) [47].

Allelic exchange and deletions were achieved using a two-step sucrose counterselection procedure with pNPTS138/pNPTS139. Insertional fusions of eGFP and mVenus were made using pGFPC-1 and pVENC-4, respectively [48]. BACTH plasmids were made using the Euromedex BACTH System Kit (Euromedex Cat. No. EUK001).

Plasmid Construction

All PCR, including insert fragments for Gibson assembly, was performed using iProof High-Fidelity DNA Polymerase (Bio-Rad Laboratories, Inc., Cat. No. 1725302) according to the manufacturer's instructions. All plasmids were constructed via Gibson assembly using NEBuilder HiFi DNA Assembly Master Mix (New England Biolabs, Inc., Cat. No. E2621X) according to the manufacturer's instructions. Prior to use in cloning, all restriction enzyme digested plasmids were treated with Calf Intestinal Alkaline Phosphatase (New England Biolabs, Inc., Cat. No. M0290S) according to the manufacturer's instructions. All primers for Gibson assembly were designed using NEBuilder Assembly Tool (New England Biolabs, Inc.). For the *bacA* complementation vector, we fused the promoter region, comprising 236 bp immediately upstream of

ABI_34190, to the coding region of *bacA* and placed the promoter/gene fusion on the low copy plasmid pMR10. The promoter/gene fusion is placed in the opposite orientation of the lacZ promoter. The restriction enzymes used are as follows for pNPTS138/pNPTS139-based vectors (*Eco*RV or *Sph*I/*Nhe*I), pET28a+ (*Sal*I/*Sac*I), pMR10 (*Eco*RV), pVENC-4 *(Nde*I/*Kpn*I), and BACTH plasmids (*Kpn*I/*Eco*RI).

Bioinformatics

Genomic and protein sequence data were obtained from the Integrated Microbial Genomes (IMG) database [49]. Multiple sequence alignment of bactofilin sequences was performed using Jalview [50] with a MAFFT alignment using the L-INS-i preset. The *C. crescentus* $BacB_{Cc}$ protein sequence used for alignment is a translation of an open reading frame in CC3022 that initiates at a downstream ATG codon, as described previously [12]. The predicted structure of *A. biprosthecum* BacA (ABI_34180) was modeled using SWISS-MODEL [51] with the structure of *C. crescentus* BacA (CC1872; PBD code 2N3D) as a template. Alignment was then processed using the ESPript server [52]. Percent identity (PID) was calculated from pairwise MAFFT alignments using the L-INS-i preset. $PID = \left(\frac{\#\ identical\ positions}{\min\ (TG_A, TG_B)}\right) \times 100$, where TG_A and TG_B are the sum of the number of residues and internal gap positions in sequences A and B in the alignment [53].

Microscopy

Light Microscopy and Fluorescence Imaging

For light microscopy analysis, cells were spotted onto pads made of 1% SeaKem LE Agarose (Lonza, Cat. No. 50000) in PYE and topped with a glass coverslip. When appropriate, the coverslip was sealed with VALAP (vaseline, lanolin, and paraffin at a 1:1:1 ratio). Images were recorded with inverted Nikon Ti-E microscopes using either 1)

a Plan Apo 60X 1.40 NA oil Ph3 DM objective with DAPI/FITC/Cy3/Cy5 or CFP/YFP/mCherry filter cubes and an iXon X3 DU885 EMCCD camera or 2) a Plan Apo λ 100X 1.45 NA oil Ph3 DM objective with DAPI/FITC/Cy3/Cy5 or CFP/YFP/mCherry filter cubes and a Photometrics Prime 95B sCMOS camera. Images were processed with NIS Elements software (Nikon). To visualize DNA, cells were grown in HIGG medium for 72h as described above. Cells were washed 1x with PYE and 1 µl of cell suspension was spotted onto a coverslip and topped with an agar pad. Cells were monitored via phase microscopy for ~1h to ensure they were growing and 20 µl of 1 mg/ml of 4',6-diamidino-2-phenylindole dihydrochloride (DAPI) was spotted on top of the agar pad. DAPI was allowed to diffuse through the pad to the cells and cells were imaged.

Structured Illumination Microscopy

3D-SIM images were collected on a DeltaVision OMX system (Applied Precision Inc., Issaquah, USA) equipped with a 1.4NA Olympus 100X oil objective. A 405 nm laser source and 419-465 nm emission filter were used for collecting HADA signal. A 488 nm laser source and 500-550 nm emission filter were used for collecting GFP signal. A 568 nm laser source and 609-654 emission filter were used for collecting TADA signal. The z-axis scanning depth was 2 µm. Immersion oil with refraction index of 1.514 was used. SIM images were reconstructed using softWoRx.

Electron Microscopy

10 µl cell or sacculi suspension was applied to an electron microscopy grid (Formvar/Carbon on 300 mesh; Ted Pella Inc., Cat. No. 01753-F) for 5 min at room temperature. Excess liquid was removed with Whatman filter paper. Cells or sacculi were then negatively stained with 10 µl 1% uranyl acetate (UA) and excess UA liquid

was immediately removed with Whatman filter paper. Grids were allowed to dry, stored in a grid holder in a desiccation chamber, and imaged with a kV JEOL JEM 1010 transmission electron microscope (JEOL USA Inc.). Protein visualization was performed as sacculi suspension except protein was applied to the grid for 1 min and stained with 2% UA before imaging.

Sacculi purification

Strains were inoculated in 3 ml PYE from colonies and grown at 26°C with shaking until late-exponential phase. Cultures were then washed 2X with ddH_2O, diluted 1:50 in HIGG, and grown at 26°C with shaking for 72h. Cells were harvested by centrifugation (7,000 g, 4°C, 15 min) and resuspended in 10 ml ddH_2O. Cell suspension was added dropwise to 20 ml boiling 7.5% SDS in a 125 ml flask with a stir bar. Once cells addition was complete, the SDS cell suspension was boiled for 30 min with stirring and then allowed to cool to room temperature. Suspension was then washed 6X with ddH_2O using centrifugation (100,000 g, 25°C, 30 min) to isolate the sacculi pellet and resuspended in 5 ml ddH_2O before imaging.

Protein purification

Recombinant plasmids overproducing His_6-BacA protein were transformed into BL21 *E. coli* strain. Transformants were grown, in LB medium supplemented with kanamycin (50 µg ml^{-1}), at 37°C until the OD_{600} = 0.6. Expression was induced by adding 0.5 mM IPTG (isopropyl β-D-thiogalactopyranoside) and incubation was continued either 3h at 30°C or overnight at 20°C. Cells pellets were resuspended in 1/25 volume of Buffer A (TrisHCl at pH 8, 300 mM NaCl, 2 mM β-mercaptoethanol) and lysed by sonication (20 sec On / 40 sec Off, 5 min, Misonix S4000). Cells debris were pelleted by centrifugation at 36,000 g for 30 min at 4°C. The supernatant was loaded on a Ni-NTA resin (Qiagen)

on an AKTA FPLC pure system. After washing with Buffer A, the protein was eluted with a linear gradient of Buffer B (50 mM TrisHCl at pH 8, 300 mM NaCl, 2 mM β-mercaptoethanol, 500 mM imidazole). Elution fraction was loaded on SDS page gel and peak fractions containing the protein were pooled. Upon purification, His_6-BacA protein was used for polymerization assay. Polymerization assay were performed by dialyzing His_6-BacA in Buffer C (25 mM TrisHCl at pH 8, 250 mM NaCl, 2 mM β-mercaptoethanol) supplemented with 10% Triton X-100 in the case of BacA.

Image analysis

Stalk length and stalk percentage data was obtained using FIJI (Fiji Is Just ImageJ) [54]. Briefly, phase micrographs were imported into FIJI and stalks were manually traced using the "Freehand Line" tool. Stalks lengths were determined from the manual trace using the "Measure" function, calibrated to the µm/pixel scale of the original micrograph. The percentage of stalked cells per image was calculated by manually counting the number of stalked and non-stalked cells per image. Subcellular localization of SpmX-eGFP and BacA-mVenus foci and subsequent localization heatmaps were generated using the ImageJ plugin MicrobeJ [55]. SpmX-eGFP maxima area and intensity were determined using the ImageJ plugin MicrobeJ [55]. Area was first generated as pixel area and converted to nm^2 based on the pixel to µm ratio for the images. Intensity is defined as the average gray value measured on the channel used to detect the particle. Analysis of BacA-mVenus time-lapse movies and BacA-mVenus foci dynamics was performed using the ImageJ plugin TrackMate [56]. All statistical analysis and data visualization was generated in R version 3.5 [57] and using the ggplot2 [58] and ggsignif [59] packages.

Cell silhouettes and cell body outlines were produced by importing the phase micrograph into Adobe Illustrator CC 2015.2.1 (Adobe Inc.) and manually tracing the silhouette or outline.

Acknowledgements

The NIH supported this work with grants 2R01GM051986 and R35GM122556 (to Y.V.B.) and GM113172 to M.S.V. and Y.V.B. Y.V.B. is also supported by a Canada 150 Research Chair in Bacterial Cell Biology. Structured illumination microscopy (3D-SIM) data acquisition was supported by NIH grant NIH1S10OD024988-01 to the Indiana University Bloomington Light Microscopy Imaging Center.

Author contributions

Conceptualization, P.D.C. and Y.V.B.; Methodology, P.D.C., M.J., and Y.V.B.; Investigation, P.D.C., with the following exception: M.J. purified and imaged the BacA proteins depicted in Figure 1E; Resources, Y.V.B. and fluorescent D-amino acids (FDAAs) from M.S.V.; Writing – Original Draft, P.D.C; Writing – Review and Editing, P.D.C., M.J., and Y.V.B.; Visualization, P.D.C.; Supervision, Y.V.B.; Funding Acquisition, Y.V.B.

Competing interests

The authors declare no competing interests.

Additional Information

All bacterial mutant strains generated during this study are available from the corresponding author upon request.

603

Table 1 – Plasmids used in this study

Plasmid	Genotype/description	Reference/source
Basic vectors		
pMR10	RK2-based, broad-host-range low copy cloning vector, Kan^R	R. Roberts and C. Mohr, unpublished
pNPTS138	sacB-containing Litmus 38 derivative suicide vector used for double homologous recombination, Kan^R	M.R.K. Alley, unpublished
pNPTS139	sacB-containing Litmus 39 derivative suicide vector used for double homologous recombination, Kan^R	M.R.K. Alley, unpublished
pGFPC-1	Integration plasmid used for creating C-terminal fusions to eGFP, $Spec/Strep^R$	[48]
pVENC-4	Integration plasmid used for creating C-terminal fusions to mVenus, $Gent^R$	[48]
pKT25	BACTH plasmid for generating in-frame fusions at the C-terminal end of the T25 fragment, Kan^R	EuroMedex
pKNT25	BACTH plasmid for generating in-frame fusions at the N-terminal end of the T25 fragment, Kan^R	EuroMedex
pUT18	BACTH plasmid for generating in-frame fusions at the N-terminal end of the T18 fragment, Amp^R	EuroMedex
pUT18C	BACTH plasmid for generating in-frame fusions at the C-terminal end of the T18 fragment, Kan^R	EuroMedex
pET28a+	His_6-tag expression vector, Kan^R	Novagen
Plasmids		
pKT25-zip	pKT25 derivative in which the leucine zipper of GCN4 yeast protein is genetically fused in frame to the T25 fragment. BACTH positive control; Kan^R	EuroMedex
pUT18C-zip	pUT18C derivative in which the leucine zipper of GCN4 yeast protein is genetically fused in frame to the T18 fragment. BACTH positive control; Amp^R	EuroMedex
pGFPC-1-$spmX_{AB}$	pGFPC-1 bearing the C-terminal fragment of *spmX* (ABI_31540); $Spec/Strep^R$	[11]
pPC10	pNPTS139 derivative used to generate a clean deletion of *bacA* (ABI_34180); Kan^R	this study
pPC21	pVENC-4 bearing the C-terminal fragment *bacA* (ABI_34180) (nt 44-543); $Gent^R$	this study
pPC36	Δ*bacA* complementation vector; pMR10 containing the promotor region upstream of the ABI_34190/ABI_34180 loci fused to the coding region of ABI_34180; Kan^R	this study
pPC62	pKT25 derivative in which SpmX is genetically fused in-frame to the T25 fragment; Kan^R	this study
pPC63	pKT25 derivative in which BacA is genetically fused in-frame to the T25 fragment; Kan^R	this study
pPC65	pKNT25 derivative in which BacA is genetically fused in-frame to the T25 fragment; Kan^R	this study
pPC67	pUT18 derivative in which SpmX is genetically fused in-frame to the T18 fragment; Amp^R	this study
pPC68	pUT18 derivative in which BacA is genetically fused in-frame to the T18 fragment; Amp^R	this study
pPC70	pUT18C derivative in which SpmX is genetically fused in-frame to the T18 fragment; Amp^R	this study
pPC72	pKNT25 derivative in which SpmX is genetically fused in-frame to the T25 fragment; Kan^R	this study
pPC73	pUT18C derivative in which BacA is genetically fused in-frame to the T18 fragment; Amp^R	this study
pMJ2	pET28a+ derivative to overexpress His-tagged $BacA_{Cc}$ (CC_1873) in *E. coli*; Kan^R	this study
pMJ4	pET28a+ derivative to overexpress His-tagged BacA (ABI_34180) in *E. coli*; Kan^R	this study
YB8246	pNPTS138-*Δ$spmX_{Ab}$*; Kan^R	[15]

604

605

Table 2 – Strains used in this study

Strain	Genotype/description	Construction	Reference/source
E. coli			
DH5α Silver Select	F^- deoR endA1 recA1 relA1 gyrA96 hsdR17(r_K^-, m_K^+) supE44 thi-1 phoA Δ(lacZYA argF)U169 Φ80lacZΔM15λ$^-$; Standard strain for cloning and maintaining plasmids	-	BioLine
BL21lDE3 (YB1000)	(F- ompT hsdSB (rB-mB-) gal dcm (lDE3); Used for protein overexpression.	-	Novagen
XL1-Blue (YB0041)	recA1, endA1, gyrA96, thi-1, hsdR17, supE44, relA1, lac [F' proAB, lacI^{q}ZΔM15, Tn10(Tet^r)]; Used for cloning and maintaining BACTH plasmids	-	Stratagene
BTH101 (YB9171)	F^-, cya-99, araD139, galE15, galK16, rpsL1 (Strr), hsdR2, mcrA1, mcrB1; Used for BACTH assays	-	EuroMedex
YB5681	DH5α strain for maintaining pGFPC-1-spmX$_{AB}$	-	[11]
YB7351	thrB1004 pro thi rpsL hsdS lacZΔM15 RP4-1360 Δ(araBAD)567 ΔdapA1341::[erm pir]; DAP (diaminopimelic acid) auxotroph used for conjugation, referred to as strain WM3064 in reference	-	[47]
YB7552	DH5α strain for maintaining pPC10	Transformation of pPC10 into DH5α	this study
YB8159	DAP auxotroph conjugative donor *E. coli* for mating plasmids into *A. biprosthecum*	Transformation of pPC10 into YB7351	this study
YB8177	DH5α strain for maintaining pPC21	Transformation of pPC21 into DH5α	this study
YB8537	DH5α strain for maintaining pMJ2	Transformation of pMJ2 into DH5α	this study
YB8539	DH5α strain for maintaining pMJ4	Transformation of pMJ4 into DH5α	this study
YB8246	DH5α strain for maintaining pNPTS138-*ΔspmX$_{Ab}$*	Transformation of pNPTS138-*ΔspmX$_{Ab}$* into DH5α	[15]
YB8552	BL21lDE3 strain containing pMJ2. For overexpression of BacA$_{Cc}$.	Transformation of pMJ2 into YB1000	this study
YB8554	BL21lDE3 strain containing pMJ4. For overexpression of BacA.	Transformation of pMJ4 into YB1000	this study
YB8584	DH5α strain for maintaining pPC36	Transformation of pPC36 into DH5α	this study
YB9158	XL1-Blue strain for maintaining pPC62	Transformation of pPC62 into YB0041	this study
YB9159	XL1-Blue strain for maintaining pPC63	Transformation of pPC63 into YB0041	this study
YB9161	XL1-Blue strain for maintaining pPC72	Transformation of pPC72 into YB0041	this study
YB9162	XL1-Blue strain for maintaining pPC65	Transformation of pPC65 into YB0041	this study
YB9164	XL1-Blue strain for maintaining pPC67	Transformation of pPC67 into YB0041	this study
YB9165	XL1-Blue strain for maintaining pPC68	Transformation of pPC68 into YB0041	this study
YB9167	XL1-Blue strain for maintaining pPC70	Transformation of pPC70 into YB0041	this study
YB9168	XL1-Blue strain for maintaining pPC73	Transformation of pPC73 into YB0041	this study
A. biprosthecum			
YB642	*A. biprosthecum* C19	-	[60]
YB5692	C19 *spmX*::*spmX-eGFP* (Spec^R/Strep^R)	Electroporation of pGFPC-1-spmX$_{AB}$ into YB642	[11]
YB7474	C19 *bacA*::*bacA-mVenus* (Gent^R)	Electroporation of pPC21 into YB642	this study
YB7487	C19 Δ*spmX bacA*::*bacA-mVenus* (Gent^R)	Electroporation of pPC21 into YB8237	this study
YB7561	C19 *spmX*::*spmX-eGFP* Δ*bacA* (Spec^R/Strep^R)	Electroporation of pGFPC-1-spmX$_{AB}$ intoYB8597	this study
YB8237	C19 Δ*spmX*	Electroporation of plasmid from YB8246 into YB642	[15]
YB8597	C19 Δ*bacA*	Mating of YB642 with YB8159	this study
YB8601	C19 Δ*bacA* / pPC36 (Kan^R)	Electroporation of pPC36 into YB8597	this study
YB8620	C19 Δ*bacA* / pMR10 (Kan^R)	Electroporation of pMR10 into YB8597	this study
YB9183	C19 / pMR10 (Kan^R)	Electroporation of pMR10 into YB642	this study

606

Table 3 – Primers used in this study

Primer ID	Sequence (5' to 3')[1]	Restriction site	Purpose
ABI_34180SeqUp	CAGGCGTTGTCTCCTTTGTC	-	Sequencing the ABI_34180 (*bacA*) locus
ABI_34180SeqDn	CGACTGGACGGTTGAAAAGG	-	
ABI_34190SeqUp	GTTAAACCTTGCGCCGTTCG	-	Sequencing the ABI_34190 locus
ABI_34190SeqDn	GGCACTGCGGTTGAGATTGA	-	
AbiBacA500C-V4F	gagacgtccaattg**catatg**AACCGACCCCGGCTCCGC	NdeI	Generation of pPC21
AbiBacA500C-V4R	tcgagatcttaa**ggtacc**CTTCAGGTCGCCCAGAGCG	KpnI	
ABI_PlmdC-bacA_F	acgccaagcttccatgggatCTACTTCAGGTCGCCCAG	-	Generation of pPC36
AbiPlytMbacA2F	CGGCGGTTATGTTCAACAAAACTAACAAACCGG	-	
AbiPlytMbacA1R	GTTGAACATAACCGCCGCCACCTAAAC	-	
ABI_PlmdC_R	gctctgcaggagatctcgatAATGTCCTTATGCAATCC	-	
delABI34180upF	aattctggatccacgatTCAATGTCGACGAAGACTTC	-	Generation of pPC10
delABI34180upR	GAGGTGGATTAGTTTTGTTGAACATAATCTCCTG	-	
delABI34180dnF	ACAAAACTAATCCACCTCACCGAACTTAATCTGTGAAGAAAGC	-	
delABI34180dnR	aagcttcctgcaggatGCGGATTCGACCGTGCCG	-	
oMJ3_BacAcc	cga**gagctc**ATGTTCAGCAAGCAAGCTAAATCG	SacI	Generation of pMJ2
oMJ4_BacAcc	taa**gtcgac**TTAGCCGGCGCTCTTGG	SalI	
oMJ5_BacAab	aga**gagctc**ATGTTCAACAAAACTAACAAACCGG	SacI	Generation of pMJ4
oMJ6_BacAab	ata**gtcgac**CTACTTCAGGTCGCCCAG	SalI	
pUT18C_AbiSpmX-F	tctagaggatccccg**ggtacc**gGTGATGAGAGCGCGTCAAAAG	KpnI	Generation of pPC62
pKT25_AbiSpmX-R	acgttgtaaaacgacggcc**gaattc**TCAGTCCTTGAGGCCGCC	EcoRI	
pKT25_AbiBacA-F	tctagaggatccccg**ggtacc**tATGTTCAACAAAACTAACAAACC	KpnI	Generation of pPC63
pKT25_AbiBacA-R	acgttgtaaaacgacggcc**gaattc**CTACTTCAGGTCGCCCAG	EcoRI	
pKTN25_AbiBacA-F	tctagaggatccccg**ggtacc**gATGTTCAACAAAACTAACAAACCGG	KpnI	Generation of pPC65
pKTN25_AbiBacA-R	cgattgctgcatggtcatt**gaattc**gaCTTCAGGTCGCCCAGAGC	EcoRI	
pUT18C_AbiSpmX-F	tctagaggatccccg**ggtacc**gGTGATGAGAGCGCGTCAAAAG	KpnI	Generation of pPC67
pUT18_AbiSpmX-R	cgtggcctcgctggcggct**gaattc**gaGTCCTTGAGGCCGCCAAG	EcoRI	
pKTN25_AbiBacA-F	tctagaggatccccg**ggtacc**gATGTTCAACAAAACTAACAAACCGG	KpnI	Generation of pPC68
pUT18_AbiBacA-R	cgtggcctcgctggcggct**gaattc**gaCTTCAGGTCGCCCAGAGC	EcoRI	
pUT18C_AbiSpmX-F	tctagaggatccccg**ggtacc**gGTGATGAGAGCGCGTCAAAAG	KpnI	Generation of pPC70
pUT18C_AbiSpmX-R	attacttagttatatcgat**gaattc**gaTCAGTCCTTGAGGCCGCC	EcoRI	
pUT18C_AbiSpmX-F	tctagaggatccccg**ggtacc**gGTGATGAGAGCGCGTCAAAAG	KpnI	Generation of pPC72
pKTN25_AbiSpmX-R	cgattgctgcatggtcatt**gaattc**gaGTCCTTGAGGCCGCCAAG	EcoRI	
pKTN25_AbiBacA-F	tctagaggatccccg**ggtacc**gATGTTCAACAAAACTAACAAACCGG	KpnI	Generation of pPC73
pUT18C_AbiBacA-R	attacttagttatatcgat**gaattc**gaCTACTTCAGGTCGCCCAG		

[1]Restriction sites in **bold**; Genomic sequence in CAPS

Figures

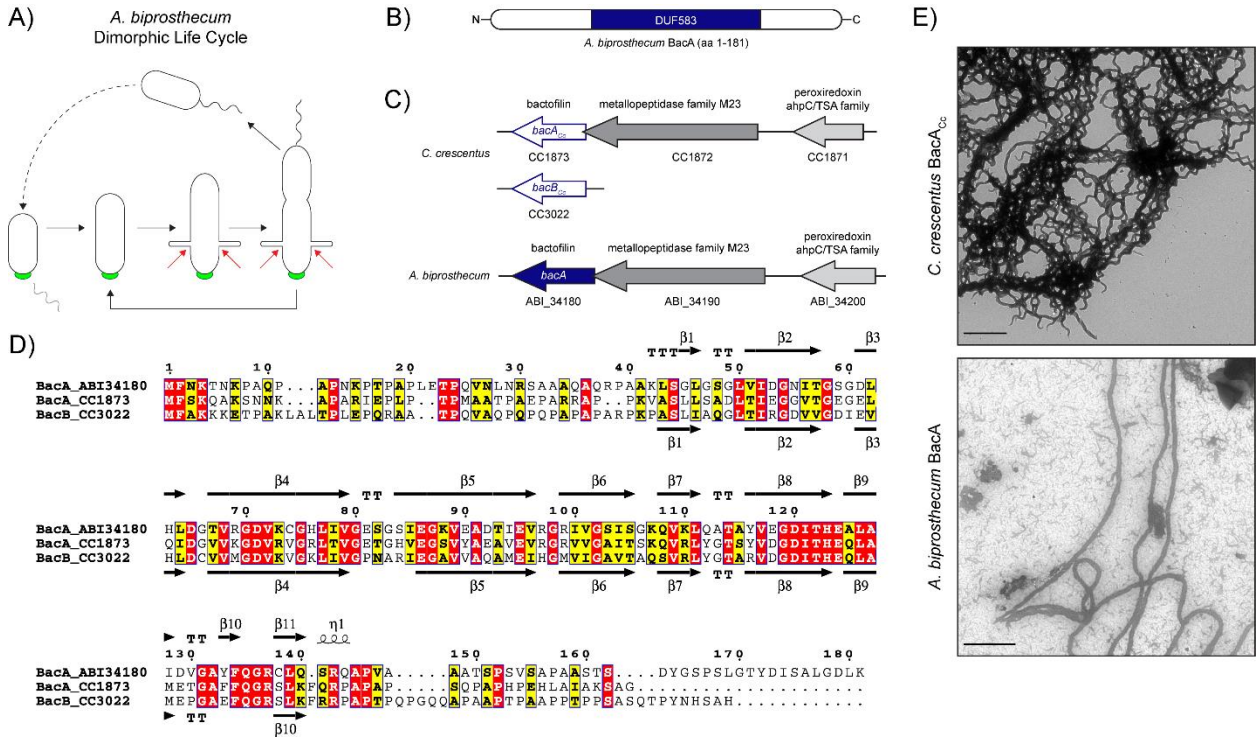

Figure 1 – Comparison of *Caulobacter crescentus* and *Asticcacaulis biprosthecum* Bactofilins

A) Dimorphic life cycle of *A. biprosthecum*. A common characteristic of prosthecate Alphaproteobacteria, the prosthecate mother cell produces an adhesive holdfast (shown in green) at one pole. Cell division results in a motile, nonreplicating swarmer cell that differentiates into a prosthecate cell. Red arrows indicate the base of *A. biprosthecum* stalks.

B) Schematic of the BacA protein from *A. biprosthecum*. The conserved bactofilin (DUF583) domain is shown in blue.

C) Schematics of the bactofilin gene loci for both *C. crescentus* and *A. biprosthecum*.

D) Alignment of *A. biprosthecum* BacA (ABI_34180) and *C. crescentus* BacA/B (CC1873/CC3022). Conserved residues are shown in red boxes, similar residues in yellow boxes with bold characters. The secondary structure of *A. biprosthecum* BacA ("BacA_ABI34180") was modeled using the SWISS-MODEL server [51] with the structure of *C. crescentus* BacA ("BacA_1873"; PBD code 2N3D) as a template [61]. The secondary structures of *C. crescentus* BacA (PDB code 2N3D) and the predicted ones for *A. biprosthecum* BacA are indicated below and above the sequence alignment, respectively. Residues are numbered according to *A. biprosthecum* BacA.

E) Transmission electron microscopy (TEM) of BacA protofilament bundles from *C. crescentus* taken in detergent free conditions (top) and *A. biprosthecum* taken in the presence of 10% Triton X-100 (bottom). Scale bars = 1 μm.

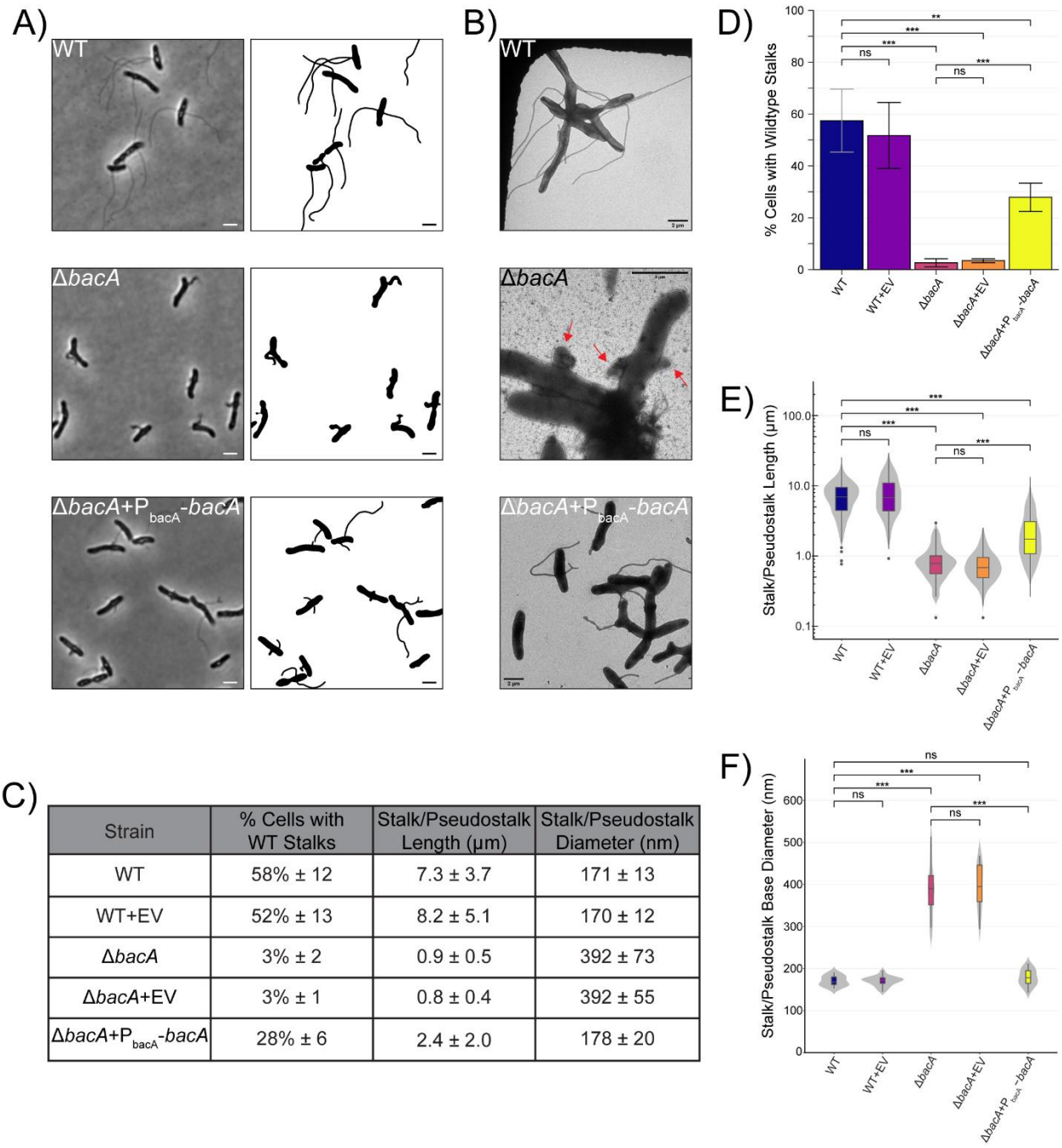

C)

Strain	% Cells with WT Stalks	Stalk/Pseudostalk Length (µm)	Stalk/Pseudostalk Diameter (nm)
WT	58% ± 12	7.3 ± 3.7	171 ± 13
WT+EV	52% ± 13	8.2 ± 5.1	170 ± 12
Δ*bacA*	3% ± 2	0.9 ± 0.5	392 ± 73
Δ*bacA*+EV	3% ± 1	0.8 ± 0.4	392 ± 55
Δ*bacA*+P_{bacA}-*bacA*	28% ± 6	2.4 ± 2.0	178 ± 20

Figure 2 – BacA is Required for WT Stalk Synthesis. Analysis of stalk morphology in strains YB642 (WT), YB9183 (WT + pMR10 empty vector control), YB8597 (Δ*bacA*), YB8620 (Δ*bacA* + pMR10 empty vector control), and YB8601 (Δ*bacA* + pMR10-P_{bacA}-*bacA*). Cells were grown in rich medium (PYE) to saturation and sub-cultured into phosphate limited (HIGG) medium at 26°C for 72h (see Methods).

A) Phase microscopy (left) and cell silhouette (right) for strains YB642 (WT), YB8597 (Δ*bacA*), and YB8601 (Δ*bacA* + pMR10-P_{bacA}-*bacA*). Scale bars = 2 µm.

B) Transmission electron microscopy (TEM) for strains YB642 (WT), YB8597 (Δ*bacA*), and YB8601 (Δ*bacA* + pMR10-P_{bacA}-*bacA*). Δ*bacA* pseudostalks are indicated with red arrows. Scale bars = 2 μm.

C) Summary statistics for data presented in Figure 2D, 2E, and 2F. Data shown is mean (SD).

D) Percentage of cells with WT stalks. Cells in phase images from Figure 2A were scored as having a WT stalk (i.e. a thin extension from the cell body). Cells exhibiting thick and aberrant pseudostalks were excluded. Data (total cells counted: WT n=735; WT+EV n=615; Δ*bacA* n=841; Δ*bacA*+EV n=1259; Δ*bacA*+ P_{bacA}-*bacA* n=831) are from four independent biological replicates with five phase microscopy fields per replicate. Data is represented as the mean (SD) percentage of cells with stalks. (***$p \leq 0.001$, **$p \leq 0.01$, ns = not significant > 0.05; two-sided t-test)

E) Distribution of stalk/pseudostalk lengths in the populations. Data (WT n=412; WT+EV n=321; Δ*bacA* n=153; Δ*bacA*+EV n=148; Δ*bacA*+ P_{bacA}-*bacA* n=324) are from three independent biological replicates with five phase microscopy fields per replicate. Data is plotted on a log10 scale y-axis and are represented as box and whisker plots [62] where the middle line represents the median, the lower and upper hinges correspond to the first and third quartiles (the 25th and 75th percentiles), and the upper whisker extends from the hinge to the largest value no further than 1.5 * IQR from the hinge (where IQR is the inter-quartile range, or distance between the first and third quartiles). The lower whisker extends from the hinge to the smallest value at most 1.5 * IQR of the hinge. Data beyond the end of the whiskers are called "outlying" points and are plotted individually. A mirrored density violin plot [63] is underlayed to show the continuous distribution of the data. As length data is approximately log-normally distributed, significant difference testing was performed on log10 transformed data (***$p \leq 0.001$, ns = not significant; two-sided t-test)

F) Distribution of stalk/pseudostalk base diameter in the populations. Data (WT n=13; WT+EV n=19; Δ*bacA* n=8; Δ*bacA*+EV n=13; Δ*bacA*+ P_{bacA}-*bacA* n= 17) are from single samples with five TEM fields per sample. Data is represented as box and whisker plots and violin plots in the same manner as Figure 2E. (***$p \leq 0.001$, ns = not significant; two-sided t-test)

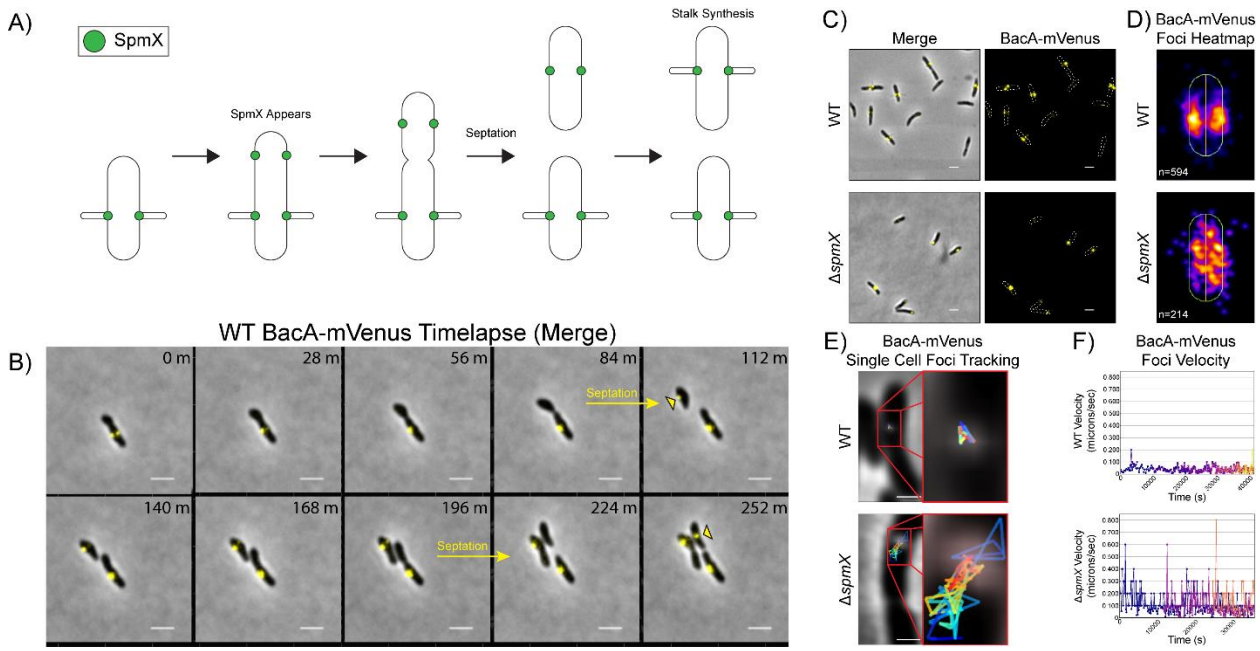

Figure 3 –BacA Localizes After Cell Division, Localizes to the Base of Stalks, and Requires SpmX for Localization. Subcellular localization of BacA-mVenus in strains YB7474 (*bacA*::*bacA-mVenus*) and YB7487 (Δ*spmX bacA*::*bacA-mVenus*) grown in rich medium (PYE) at 26°C for 24-48h.

A) Model of cell-cycle timing of SpmX localization. Previous work [11] has shown that SpmX appears in predivisional cells and marks the sites of stalks synthesis prior to cell division.

B) Time lapse microscopy montage showing the dynamics of BacA-mVenus localization in strain YB7474 (*bacA*::*bacA-mVenus*). Frames show images taken every 28 minutes. Yellow arrows and text show the transition from pre-septation to post-septation. Yellow black-bordered triangles mark the appearance of new BacA-mVenus foci in recently divided daughter cells. Scale bars = 2 µm

C) BacA-mVenus subcellular localization. Phase merge and fluorescence microscopy images. Scale bars = 2 µm.

D) Population level heatmaps of BacA-mVenus subcellular localization. Number of cells analyzed is shown on the bottom left of each heatmap.

E) Single cell BacA-mVenus foci tracking. Tracks are colored by time, with blue representing the earliest timepoints and red representing the latest time points. Scale bars = 1 µm.

F) Velocity tracking of multiple BacA-mVenus foci from time-lapse movies. Particle tracking was performed and velocity (µm/s) from frame-to-frame for each focus was calculated. Each color represents the track of individual foci as they appear.

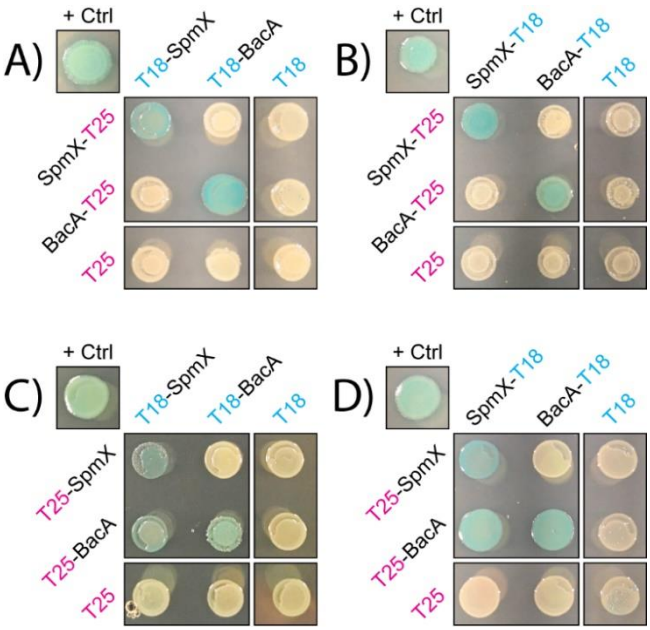

Figure 4 – Bacteria Adenylate Cyclase Two-Hybrid (BACTH) Assays Showing *in vivo* Interaction of SpmX and BacA. BTH101 *E. coli* were co-transformed with T25 and T18 based recombinant plasmids. Transformants were then grown in selective medium containing 0.5 mM IPTG and patched on selective indicator plates containing X-gal 40 µg ml^{-1} and 0.5 mM IPTG for ~24 hours at 30°C (see Methods). As this is a β-galactosidase assay, blue patches indicate a positive *in vivo* interaction between the two recombinant proteins. Positive control ("+ Crtl") for all assays is T25-Zip and T18-Zip fusion proteins. Negative controls are unfused T18 or T25 fragments in combination with the experimental fusion protein or the cognate unfused T25 or T18 fragments. Patches shown are representative of independent biological triplicates for each combination.

A) C-terminal fused T25 + N-terminal fused T18

B) C-terminal fused T25 + C-terminal fused T18

C) N-terminal fused T25 + N-terminal fused T18

D) N-terminal fused T25 + C-terminal fused T18

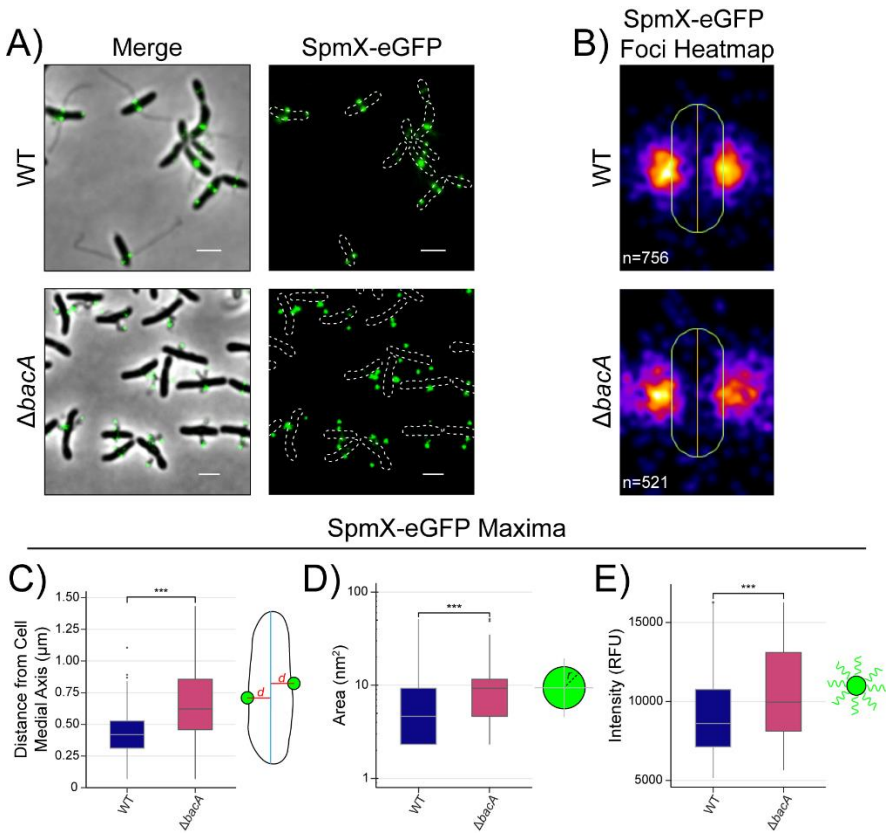

Figure 5 – BacA is Required to Stabilize SpmX-eGFP at the Base of the Stalk and to Constrain the Size of SpmX-eGFP Maxima. Subcellular localization of SpmX-eGFP in strains YB5692 (*spmX*::*spmX-eGFP*; top row) and YB7561 (*spmX*::*spmX-eGFP* Δ*bacA*; bottom row). Cells were grown in rich medium (PYE) to saturation and sub-cultured into phosphate limited (HIGG) medium at 26°C for 72h (see Methods).

A) Phase merge and fluorescence microscopy images. Scale bars = 2 µm.

B) Population level heatmaps of SpmX-eGFP subcellular localization. Data (WT n=756; Δ*bacA* n=521) are from three independent biological replicates with five microscopy fields per replicate.

C) Distribution of orthogonal distance (µm) of each SpmX-eGFP maxima from the medial axis of its associated parent cell. Data set is the same as used in Figure 6B. Data is plotted on a continuous y-axis and are represented as box and whisker plots as described in Figure 2E. (***$p \leq 0.001$; two-sided t-test)

D) Distribution of SpmX-eGFP maxima area (nm^2) in the populations. Data set is the same as used in Figure 6B. Data is plotted on a log_{10} scale y-axis and are represented as box and whisker plots as described in Figure 2E. (***$p \leq 0.001$; two-sided t-test)

E) Distribution of SpmX-eGFP maxima fluorescence intensity (relative fluorescence units; RFU) in the populations. Data set is the same as used in Figure 6B. Data is plotted on a continuous y-axis and are represented as box and whisker plots as described in Figure 2E. (***$p \leq 0.001$; two-sided t-test)

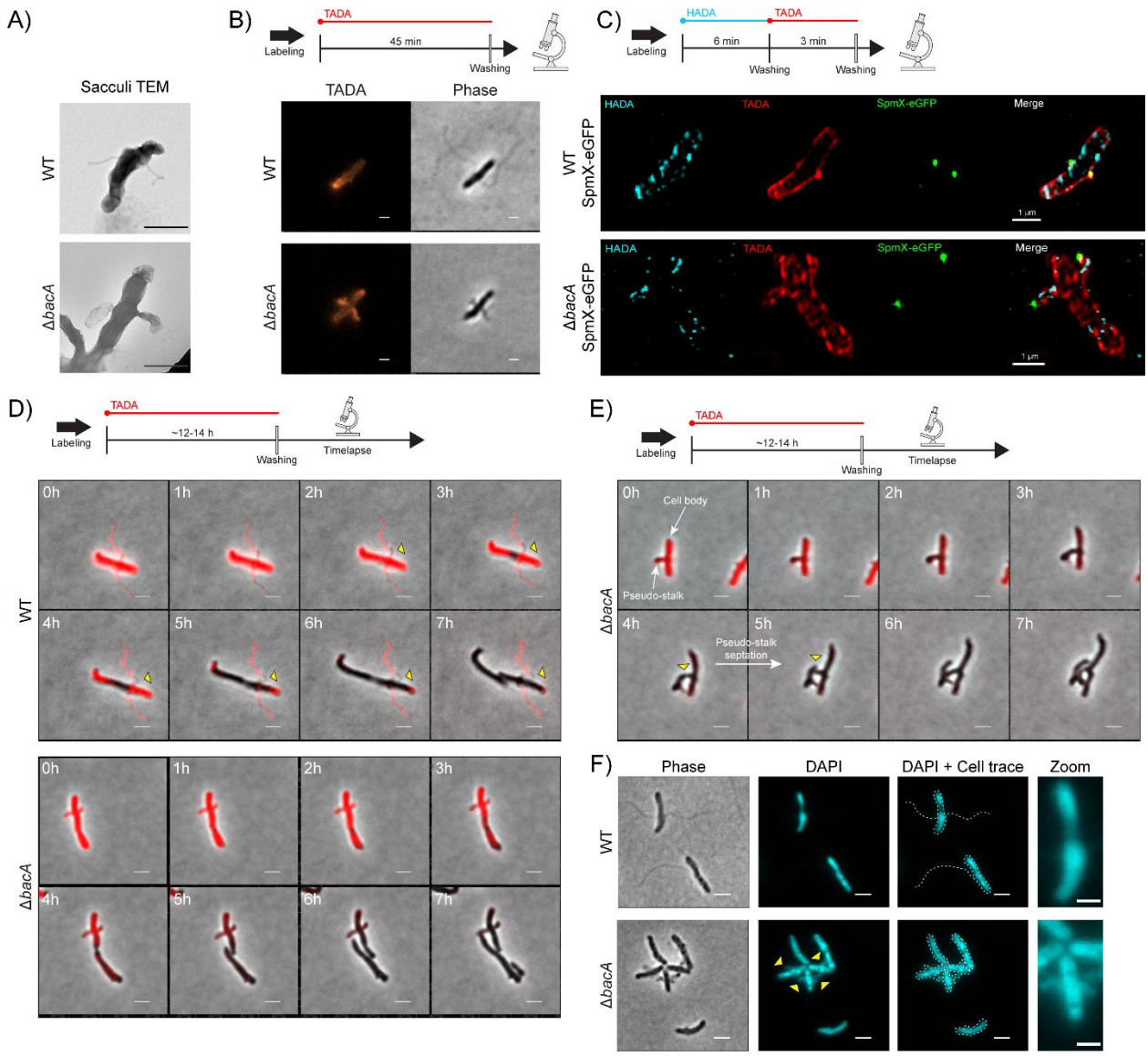

Figure 6 – Peptidoglycan (PG) Composition & Remodeling and Septation & DNA Content in WT Stalks and Δ*bacA* Pseudostalks.

A) Transmission electron microscopy (TEM) of prepared PG sacculi for strains YB642 (WT) and YB8597 (Δ*bacA*). Cells were grown in rich medium (PYE) to saturation and sub-cultured into phosphate limited (HIGG) medium at 26°C for 72h (see Methods) before preparing sacculi. Sacculi were prepared by boiling in SDS for 30 minutes followed by washing ≥6X with dH_2O. Scale bars = 1 µm

B) Medium pulse FDAA (TADA) labeling showing active PG remodeling in strains YB642 (WT) and YB8597 (Δ*bacA*). Cells were grown in rich medium (PYE) to saturation and sub-cultured into phosphate limited (HIGG) medium at 26°C for 72h (see Methods) before labeling. Cells were washed with 2X PYE, labeled with 500 µM TADA for 45 minutes, washed 2X with PYE, and imaged with phase and fluorescence microscopy. Representative images are shown. Scale bars = 2 µm.

C) Virtual time lapse: Short pulse, sequential, dual FDAA (TADA and HADA) labeling showing active PG remodeling in strains YB5692 (*spmX*::*spmX-eGFP*) and YB7561 (*spmX*::*spmX-eGFP* Δ*bacA*). Cells were grown in rich medium (PYE) to saturation and sub-cultured into phosphate limited (HIGG) medium at 26°C for 72h (see Methods) before labeling. Cells were washed 2X with PYE, labeled with 500 μM HADA for 6 minutes, washed 2X with PYE, labeled with 500 μM TADA for 3 minutes, washed 2X with PYE, and imaged via 3D-SIM (Structured Illumination Microscopy). Representative images are shown. Scale bars = 1 μm.

D) Pulse-chase time-lapse of FDAA (TADA) labeling for strains YB642 (WT) and YB8597 (Δ*bacA*) showing loss of labeling as peptidoglycan is actively remodeled. Yellow triangles with black outline indicate loss of TADA signal in YB642 (WT) as stalk is extended from the base. Cells were grown in rich medium (PYE) to saturation and sub-cultured into phosphate limited (HIGG) medium at 26°C for 60h (see Methods) before labeling. To label whole cells, 250 μM TADA was added and cells were allowed to grow an additional ~12-14h (overnight). Cells were then washed 2X with PYE to remove TADA and imaged via time-lapse with phase and fluorescence microscopy. Scale bars = 2 μm.

E) Pulse-chase time-lapse of FDAA (TADA) labeling for strains YB8597 (Δ*bacA*) showing elongation and septation of a pseudo-stalk. Yellow triangles with black outline indicate the septation site. Cells were grown as described in Figure 7D. Scale bars = 2 μm.

F) DAPI staining for DNA in strains YB642 (WT) and YB8597 (Δ*bacA*) showing DNA is present in the pseudo stalk (yellow triangles). Representative images are shown. Scale bars = 2 μm.

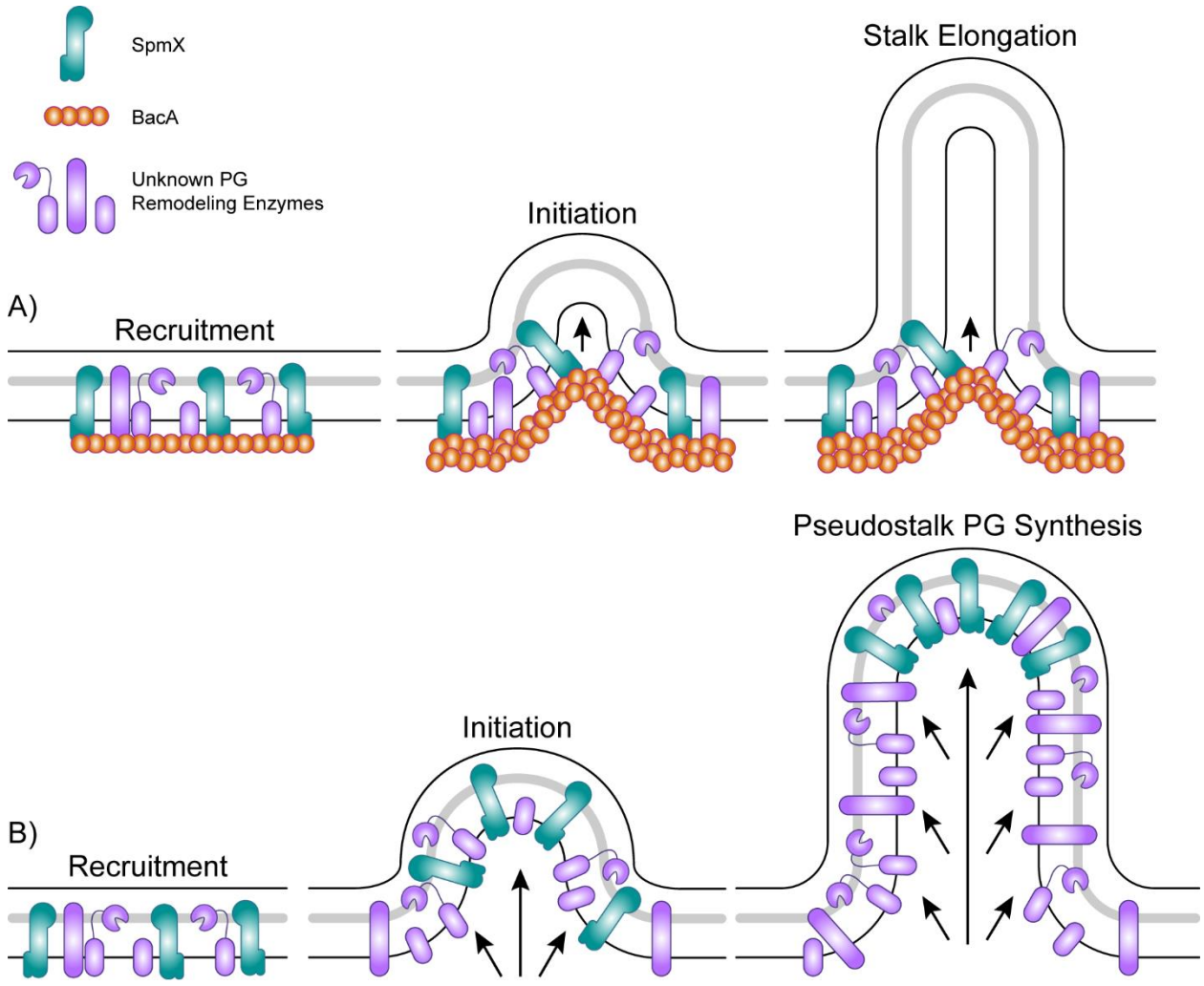

Figure 7 – Model of the Stalk PG Biosynthetic Complex in *A. biprosthecum*.

A) Model of *A. biprosthecum* WT stalk synthesis. SpmX recruits the PG remodeling complex and the BacA scaffold to the site of stalk synthesis (left). PG synthesis is initiated at the site defined by SpmX localization and in an area constrained by BacA (middle). As PG synthesis progresses and the stalk elongates, synthesis is constrained at the base of the stalk by the BacA scaffold (right).

B) Model of *A. biprosthecum* Δ*bacA* pseudostalk synthesis. As with WT cells, SpmX recruits the PG remodeling complex to the site of stalk synthesis (left). PG synthesis is initiated at the site defined by SpmX localization (middle). As PG synthesis progresses, there is no BacA scaffold to constrain the complex at the base of the synthesis site: PG synthesis occurs promiscuously throughout, with SpmX localized to the distal end of the structure (right), leading to short, wide pseudostalks.

Protein	*C. crescentus*		*A. biprosthecum*	
	Role in stalk synthesis	Loss of function phenotype	Role in stalk synthesis	Loss of function phenotype
BacA [12]	• Cytoskeletal protein • Localizes PbpC to stalked pole	• Shorter stalks under phosphate starvation • PbpC does not localize	Unknown at time of study initiation	Unknown at time of study initiation
BacB [12]	• Cytoskeletal protein • Localizes PbpC to stalked pole	• Shorter stalks under phosphate starvation • PbpC does not localize	No homolog	N/A
PbpC [12, 26]	• Class A (bifunctional) PBP • Localizes StpX to stalked pole	• Shorter stalks under phosphate starvation • StpX does not localize	No homolog	N/A
StpX [25, 26]	• Potential role in metal homeostasis	• Shorter stalks under phosphate starvation	No homolog	N/A
SpmX [11, 64]	• None (involved in regulation of asymmetric cell division)	• Division defects	• Required for stalk synthesis • Marks site of stalk synthesis	• Stalkless cells

Supplemental Table 1 – Proteins involved in stalk synthesis. At the time this study was initiated, four *C. crescentus proteins* (BacA, BacB, PbpC, and StpX) had been shown to be involved in stalk synthesis. Of these four, only one (BacA) had a bi-directional best hit homolog in *A. biprosthecum*. The one *A. biprosthecum* protein involved in stalk synthesis (SpmX) has a *C. crescentus* homolog, but in *C. crescentus* this protein is involved in cell cycle regulation and not stalk synthesis.

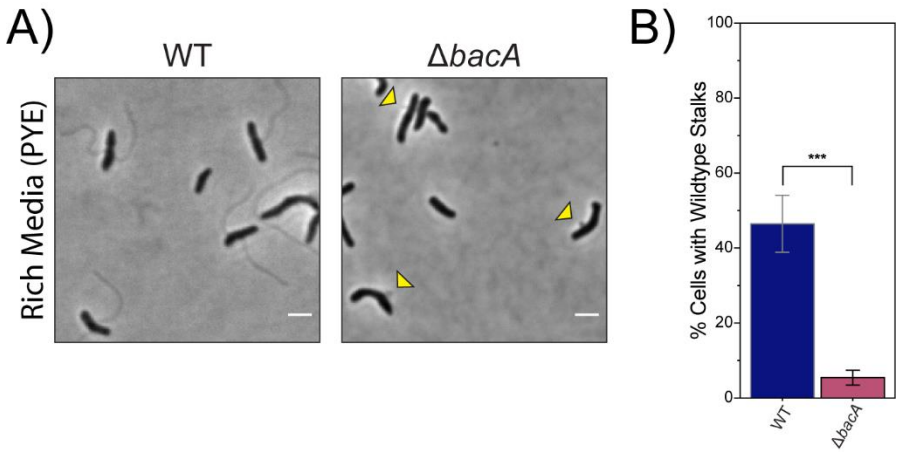

Supplemental Figure 1 – *A. biprosthecum* stalk phenotypes in rich medium (PYE). Analysis of stalk phenotype in strains YB642 (WT) and YB8597 (Δ*bacA*). Cells were grown in rich medium (PYE) at 26°C for 48h.

A) Phase microscopy for strains YB642 (WT) and YB8597 (Δ*bacA*). Scale bars = 2 µm.

B) Percentage of cells with WT stalks. Cells in phase images from Figure S1A were scored as having a WT stalk (i.e. a thin extension from the cell body). Yellow triangles indicate Δ*bacA* midcell protrusions. Data (total cells counted: WT n=747; Δ*bacA* n=577) are from four independent biological replicates with five phase microscopy fields per replicate. Data is represented as the mean (SD) percentage of cells with stalks. (***$p \leq 0.001$; two-sided t-test)

References

1. Young, K.D. (2006). The selective value of bacterial shape. Microbiol Mol Biol Rev *70*, 660-703.

2. Justice, S.S., Hunstad, D.A., Cegelski, L., and Hultgren, S.J. (2008). Morphological plasticity as a bacterial survival strategy. Nature reviews. Microbiology *6*, 162-168.

3. Caccamo, P.D., and Brun, Y.V. (2018). The Molecular Basis of Noncanonical Bacterial Morphology. Trends in microbiology *26*, 191-208.

4. Horvath, D.J., Jr., Li, B., Casper, T., Partida-Sanchez, S., Hunstad, D.A., Hultgren, S.J., and Justice, S.S. (2011). Morphological plasticity promotes resistance to phagocyte killing of uropathogenic Escherichia coli. Microbes Infect *13*, 426-437.

5. Perez-Nunez, D., Briandet, R., David, B., Gautier, C., Renault, P., Hallet, B., Hols, P., Carballido-Lopez, R., and Guedon, E. (2011). A new morphogenesis pathway in bacteria: unbalanced activity of cell wall synthesis machineries leads to coccus-to-rod transition and filamentation in ovococci. Mol Microbiol *79*, 759-771.

6. Khandige, S., Asferg, C.A., Rasmussen, K.J., Larsen, M.J., Overgaard, M., Andersen, T.E., and Moller-Jensen, J. (2016). DamX Controls Reversible Cell Morphology Switching in Uropathogenic Escherichia coli. MBio *7*.

7. Flardh, K., Richards, D.M., Hempel, A.M., Howard, M., and Buttner, M.J. (2012). Regulation of apical growth and hyphal branching in *Streptomyces*. Curr Opin Microbiol *15*, 737-743.

8. Wagner, J.K., Setayeshgar, S., Sharon, L.A., Reilly, J.P., and Brun, Y.V. (2006). A nutrient uptake role for bacterial cell envelope extensions. Proc Natl Acad Sci U S A *103*, 11772-11777.

9. Wagner, J.K., and Brun, Y.V. (2007). Out on a limb: how the Caulobacter stalk can boost the study of bacterial cell shape. Mol Microbiol *64*, 28-33.

10. Abraham, W.-R., Rohde, M., and Bennasar, A. (2014). The Family Caulobacteraceae. In The Prokaryotes: Alphaproteobacteria and Betaproteobacteria, E. Rosenberg, E.F. DeLong, S. Lory, E. Stackebrandt and F. Thompson, eds. (Berlin, Heidelberg: Springer Berlin Heidelberg), pp. 179-205.

11. Jiang, C., Brown, P.J., Ducret, A., and Brun, Y.V. (2014). Sequential evolution of bacterial morphology by co-option of a developmental regulator. Nature *506*, 489-493.

12. Kuhn, J., Briegel, A., Morschel, E., Kahnt, J., Leser, K., Wick, S., Jensen, G.J., and Thanbichler, M. (2010). Bactofilins, a ubiquitous class of cytoskeletal proteins mediating polar localization of a cell wall synthase in *Caulobacter crescentus*. EMBO J *29*, 327-339.

13. Sycuro, L.K., Pincus, Z., Gutierrez, K.D., Biboy, J., Stern, C.A., Vollmer, W., and Salama, N.R. (2010). Peptidoglycan crosslinking relaxation promotes *Helicobacter pylori*'s helical shape and stomach colonization. Cell *141*, 822-833.

14. Jackson, K.M., Schwartz, C., Wachter, J., Rosa, P.A., and Stewart, P.E. (2018). A widely conserved bacterial cytoskeletal component influences unique helical shape and motility of the spirochete *Leptospira biflexa*. Mol Microbiol *108*, 77-89.

15. Randich, A.M., Kysela, D.T., Morlot, C., and Brun, Y.V. (2019). Origin of a Core Bacterial Gene via Co-option and Detoxification of a Phage Lysin. Curr Biol *29*, 1634-1646 e1636.

16. Brun, Y.V., and Shapiro, L. (1992). A temporally controlled sigma-factor is required for polar morphogenesis and normal cell division in Caulobacter. Genes Dev *6*, 2395-2408.

17. Biondi, E.G., Skerker, J.M., Arif, M., Prasol, M.S., Perchuk, B.S., and Laub, M.T. (2006). A phosphorelay system controls stalk biogenesis during cell cycle progression in Caulobacter crescentus. Mol Microbiol *59*, 386-401.

18. Schmidt, J.M., and Stanier, R.Y. (1966). The development of cellular stalks in bacteria. J Cell Biol *28*, 423-436.

19. Gonin, M., Quardokus, E.M., O'Donnol, D., Maddock, J., and Brun, Y.V. (2000). Regulation of stalk elongation by phosphate in *Caulobacter crescentus*. Journal of bacteriology *182*, 337-347.

20. Curtis, P.D. (2017). Stalk formation of Brevundimonas and how it compares to Caulobacter crescentus. PloS one *12*, e0184063.

21. Lawler, M.L., and Brun, Y.V. (2007). Advantages and mechanisms of polarity and cell shape determination in Caulobacter crescentus. Curr Opin Microbiol *10*, 630-637.

22. Thanbichler, M. (2009). Spatial regulation in Caulobacter crescentus. Curr Opin Microbiol *12*, 715-721.

23. Brown, P.J., Hardy, G.G., Trimble, M.J., and Brun, Y.V. (2009). Complex regulatory pathways coordinate cell-cycle progression and development in Caulobacter crescentus. Adv Microb Physiol *54*, 1-101.

24. Sundararajan, K., and Goley, E.D. (2017). Cytoskeletal Proteins in Caulobacter crescentus: Spatial Orchestrators of Cell Cycle Progression, Development, and Cell Shape. Subcell Biochem *84*, 103-137.

25. Hughes, H.V., Huitema, E., Pritchard, S., Keiler, K.C., Brun, Y.V., and Viollier, P.H. (2010). Protein localization and dynamics within a bacterial organelle. Proc Natl Acad Sci U S A *107*, 5599-5604.

26. Hughes, H.V., Lisher, J.P., Hardy, G.G., Kysela, D.T., Arnold, R.J., Giedroc, D.P., and Brun, Y.V. (2013). Co-ordinate synthesis and protein localization in a bacterial organelle by the action of a penicillin-binding-protein. Mol Microbiol *90*, 1162-1177.

27. Vasa, S., Lin, L., Shi, C., Habenstein, B., Riedel, D., Kuhn, J., Thanbichler, M., and Lange, A. (2015). beta-Helical architecture of cytoskeletal bactofilin filaments revealed by solid-state NMR. Proc Natl Acad Sci U S A *112*, E127-136.

28. Karimova, G., Pidoux, J., Ullmann, A., and Ladant, D. (1998). A bacterial two-hybrid system based on a reconstituted signal transduction pathway. Proc Natl Acad Sci U S A *95*, 5752-5756.

29. Perez, A.M., Mann, T.H., Lasker, K., Ahrens, D.G., Eckart, M.R., and Shapiro, L. (2017). A Localized Complex of Two Protein Oligomers Controls the Orientation of Cell Polarity. MBio *8*.

30. Deng, X., Gonzalez Llamazares, A., Wagstaff, J.M., Hale, V.L., Cannone, G., McLaughlin, S.H., Kureisaite-Ciziene, D., and Lowe, J. (2019). The structure of bactofilin filaments reveals their mode of membrane binding and lack of polarity. Nat Microbiol.

31. den Blaauwen, T., de Pedro, M.A., Nguyen-Disteche, M., and Ayala, J.A. (2008). Morphogenesis of rod-shaped sacculi. FEMS Microbiol Rev *32*, 321-344.

32. Kuru, E., Hughes, H.V., Brown, P.J., Hall, E., Tekkam, S., Cava, F., de Pedro, M.A., Brun, Y.V., and VanNieuwenhze, M.S. (2012). In Situ probing of newly synthesized peptidoglycan in live bacteria with fluorescent D-amino acids. Angew Chem Int Ed Engl *51*, 12519-12523.

33. Brown, P.J., Kysela, D.T., and Brun, Y.V. (2011). Polarity and the diversity of growth mechanisms in bacteria. Semin Cell Dev Biol *22*, 790-798.

34. Pinho, M.G., Kjos, M., and Veening, J.W. (2013). How to get (a)round: mechanisms controlling growth and division of coccoid bacteria. Nature reviews. Microbiology *11*, 601-614.

35. Wali, T.M., Hudson, G.R., Danald, D.A., and Weiner, R.M. (1980). Timing of swarmer cell cycle morphogenesis and macromolecular synthesis by

Hyphomicrobium neptunium in synchronous culture. Journal of bacteriology *144*, 406-412.

36. Moore, R.L. (1981). The biology of *Hyphomicrobium* and other prosthecate, budding bacteria. Annu Rev Microbiol *35*, 567-594.

37. Zerfas, P.M., Kessel, M., Quintero, E.J., and Weiner, R.M. (1997). Fine-structure evidence for cell membrane partitioning of the nucleoid and cytoplasm during bud formation in Hyphomonas species. Journal of bacteriology *179*, 148-156.

38. Cserti, E., Rosskopf, S., Chang, Y.W., Eisheuer, S., Selter, L., Shi, J., Regh, C., Koert, U., Jensen, G.J., and Thanbichler, M. (2017). Dynamics of the peptidoglycan biosynthetic machinery in the stalked budding bacterium *Hyphomonas neptunium*. Mol Microbiol *103*, 875-895.

39. Meniche, X., Otten, R., Siegrist, M.S., Baer, C.E., Murphy, K.C., Bertozzi, C.R., and Sassetti, C.M. (2014). Subpolar addition of new cell wall is directed by DivIVA in mycobacteria. Proc Natl Acad Sci U S A *111*, E3243-3251.

40. Melzer, E.S., Sein, C.E., Chambers, J.J., and Sloan Siegrist, M. (2018). DivIVA concentrates mycobacterial cell envelope assembly for initiation and stabilization of polar growth. Cytoskeleton (Hoboken) *75*, 498-507.

41. Kysela, D.T., Randich, A.M., Caccamo, P.D., and Brun, Y.V. (2016). Diversity Takes Shape: Understanding the Mechanistic and Adaptive Basis of Bacterial Morphology. PLoS Biol *14*, e1002565.

42. Taylor, J.A., Sichel, S.R., and Salama, N.R. (2019). Bent Bacteria: A Comparison of Cell Shape Mechanisms in Proteobacteria. Annu Rev Microbiol *73*, 457-480.

43. Poindexter, J.S. (1978). Selection for nonbuoyant morphological mutants of Caulobacter crescentus. Journal of bacteriology *135*, 1141-1145.

44. Dower, W.J., Miller, J.F., and Ragsdale, C.W. (1988). High efficiency transformation of E. coli by high voltage electroporation. Nucleic acids research *16*, 6127-6145.

45. Chung, C.T., Niemela, S.L., and Miller, R.H. (1989). One-step preparation of competent Escherichia coli: transformation and storage of bacterial cells in the same solution. Proc Natl Acad Sci U S A *86*, 2172-2175.

46. Chung, C.T., and Miller, R.H. (1993). Preparation and storage of competent Escherichia coli cells. Methods Enzymol *218*, 621-627.

47. Saltikov, C.W., and Newman, D.K. (2003). Genetic identification of a respiratory arsenate reductase. Proc Natl Acad Sci U S A *100*, 10983-10988.

48. Thanbichler, M., Iniesta, A.A., and Shapiro, L. (2007). A comprehensive set of plasmids for vanillate- and xylose-inducible gene expression in Caulobacter crescentus. Nucleic acids research *35*, e137.

49. Chen, I.A., Chu, K., Palaniappan, K., Pillay, M., Ratner, A., Huang, J., Huntemann, M., Varghese, N., White, J.R., Seshadri, R., et al. (2019). IMG/M v.5.0: an integrated data management and comparative analysis system for microbial genomes and microbiomes. Nucleic acids research *47*, D666-D677.

50. Waterhouse, A.M., Procter, J.B., Martin, D.M., Clamp, M., and Barton, G.J. (2009). Jalview Version 2--a multiple sequence alignment editor and analysis workbench. Bioinformatics *25*, 1189-1191.

51. Waterhouse, A., Bertoni, M., Bienert, S., Studer, G., Tauriello, G., Gumienny, R., Heer, F.T., de Beer, T.A.P., Rempfer, C., Bordoli, L., et al. (2018). SWISS-MODEL: homology modelling of protein structures and complexes. Nucleic acids research *46*, W296-W303.

52. Robert, X., and Gouet, P. (2014). Deciphering key features in protein structures with the new ENDscript server. Nucleic acids research *42*, W320-324.

53. Raghava, G.P., and Barton, G.J. (2006). Quantification of the variation in percentage identity for protein sequence alignments. BMC Bioinformatics *7*, 415.

54. Schindelin, J., Arganda-Carreras, I., Frise, E., Kaynig, V., Longair, M., Pietzsch, T., Preibisch, S., Rueden, C., Saalfeld, S., Schmid, B., et al. (2012). Fiji: an open-source platform for biological-image analysis. Nat Methods *9*, 676-682.

55. Ducret, A., Quardokus, E.M., and Brun, Y.V. (2016). MicrobeJ, a tool for high throughput bacterial cell detection and quantitative analysis. Nat Microbiol *1*, 16077.

56. Tinevez, J.Y., Perry, N., Schindelin, J., Hoopes, G.M., Reynolds, G.D., Laplantine, E., Bednarek, S.Y., Shorte, S.L., and Eliceiri, K.W. (2017). TrackMate: An open and extensible platform for single-particle tracking. Methods *115*, 80-90.

57. R Development Core Team (2012). R: a language and environment for statistical computing. (Vienna, Austria: The R Foundation for Statistical Computing).

58. Wickham, H. (2016). ggplot2: Elegant Graphics for Data Analysis. (New York: Springer-Verlag).

59. Ahlmann-Eltze, C. (2019). ggsignif: Significance Brackets for 'ggplot2'. 0.5.0 Edition.

60. Pate, J.L., and Ordal, E.J. (1965). The fine structure of two unusual stalked bacteria. J Cell Biol *27*, 133-150.

61. Shi, C., Fricke, P., Lin, L., Chevelkov, V., Wegstroth, M., Giller, K., Becker, S., Thanbichler, M., and Lange, A. (2015). Atomic-resolution structure of cytoskeletal bactofilin by solid-state NMR. Sci Adv *1*, e1501087.

62. Mcgill, R., Tukey, J.W., and Larsen, W.A. (1978). Variations of Box Plots. Am Stat *32*, 12-16.

63. Hintze, J.L., and Nelson, R.D. (1998). Violin Plots: A Box Plot-Density Trace Synergism. The American Statistician *52*, 181-184.

64. Radhakrishnan, S.K., Thanbichler, M., and Viollier, P.H. (2008). The dynamic interplay between a cell fate determinant and a lysozyme homolog drives the asymmetric division cycle of *Caulobacter crescentus*. Genes Dev *22*, 212-225.